



저작자표시-비영리-변경금지 2.0 대한민국

이용자는 아래의 조건을 따르는 경우에 한하여 자유롭게

- 이 저작물을 복제, 배포, 전송, 전시, 공연 및 방송할 수 있습니다.

다음과 같은 조건을 따라야 합니다:



저작자표시. 귀하는 원저작자를 표시하여야 합니다.



비영리. 귀하는 이 저작물을 영리 목적으로 이용할 수 없습니다.



변경금지. 귀하는 이 저작물을 개작, 변형 또는 가공할 수 없습니다.

- 귀하는, 이 저작물의 재이용이나 배포의 경우, 이 저작물에 적용된 이용허락조건을 명확하게 나타내어야 합니다.
- 저작권자로부터 별도의 허가를 받으면 이러한 조건들은 적용되지 않습니다.

저작권법에 따른 이용자의 권리는 위의 내용에 의하여 영향을 받지 않습니다.

이것은 [이용허락규약\(Legal Code\)](#)을 이해하기 쉽게 요약한 것입니다.

[Disclaimer](#)

Thesis for the Degree of Master of Engineering

Au Nanoparticle-Based Composites for Triboelectric Nanogenerator and Photocatalysis Applications



by

Merreta Noorenza Biutty

Department of Polymer Engineering

The Graduate School

Pukyong National University

February 21, 2020

Au Nanoparticle-Based Composites for Triboelectric Nanogenerator and Photocatalysis Applications

금 나노입자 기반 복합체를 활용한 마찰전기 나노발전기
및 광촉매 연구

Advisor: Prof. Seong Il Yoo

by

Merreta Noorenza Biutty

A thesis submitted in partial fulfillment of the requirements
for the degree of

Master of Engineering

in Department of Polymer Engineering, The Graduate School,
Pukyong National University

February 2020

Au Nanoparticle-Based Composites for Triboelectric Nanogenerator and Photocatalysis Applications

A dissertation

by

Merreta Noorenza Biutty

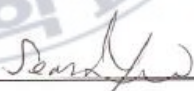
Approved by:



Prof. Joo Hyun Kim



Prof. U Hyeok Choi



Prof. Seong Il Yoo

February 21, 2020

CONTENTS

Content.....	i
List of Tables.....	v
List of Figures	vi
Abstract	x
Chapter I. Introduction	1
I-1. Energy Harvesting	1
I-2. Triboelectric Nanogenerator (TENG)	2
I-2.1. Vertical-contact Separation of TENG	2
I-2.2. Improving of TENG	4
I-2.2.1. Material Selection	4
I-2.2.2. Surface Physical Modification	5
I-2.2.3. Surface Chemical Modification	6
I-3. Mussel-Inspired Polydopamine Coating	6
I-4. Metal Nanoparticle	7

I-4.1. Localized Surface Plasmon Resonance	8
I-4.2. Plasmonic Coupling	10
I-5. Photocatalysis	12
I-5.1. Semiconductor Photocatalysis	12
I-5.2. Metal-Semiconductor Photocatalysis	12
I-5.3. Hot-Electron Injection	13
Chapter II. Au Nanoparticles-embedded Porous PDMS Composites for Triboelectric Nanogenerator with Enhanced Performance	14
II-1. Introduction.....	14
II-2. Experimental Section.....	16
II-2.1. Material	16
II-2.2. Procedure	16
II-2.2.1. Fabrication of PDMS Sponge	16
II-2.2.2. Synthesis of Gold Nanoparticle	17
II-2.2.3. Modification of PDMS Sponge.....	17

II-2.2.4. Fabrication of TENG.....	18
II-2.3. Measurement	18
II-3. Result and Discussion	19
II-3.1. Characteristic of PDMS Sponge and Gold Nanoparticles	19
II-3.2. Characteristic of PDMS Sponge/PDA/Au	22
II-3.3. Comparison Performance of Triboelectric Nanogenerator	25
II-3.4. Contribution Material Inside of Pore	31
II-3.5. Optimum Condition of Triboelectric Nanogenerator Performance	33
II-4. Conclusion	35
Chapter III. Synthesis of Chain-like Au@TiO₂ and Their Photocatalytic Activity.....	36
III-1. Introduction	36
III-2. Experimental Section.....	38
III-2.1. Material	38
III-2.2. Procedure	38

III-2.2.1. Synthesis of Gold Nanoparticles	38
III-2.2.2. Synthesis of Isolated and Chain-like Au@TiO ₂	39
III-2.2.3. Photocatalytic Activity	39
III-2.3. Measurement	39
III-3. Result and Discussion.....	40
III-3.1. Linear Aggregation of Gold Nanoparticle	40
III-3.2. Synthesis and Characteristic of Isolated and Chain-like Au@TiO ₂	45
III-3.3. Photocatalytic Activity	48
III-4. Conclusion.....	59
References	60
Acknowledgment	68

LIST OF TABLES

Table 1. Comparison of various energy harvesting technologies

Table 2. Triboelectric series



LIST OF FIGURES

- Figure 1. Simple mechanism of vertical contact-separation of TENG.
- Figure 2. Schematic diagram of localized surface-plasmon resonance (LSPR) process.
- Figure 3. Plasmonic coupling (A, B) Near field enhancement distribution produced by a silver spherical NP with $D = 25$ nm and by a pair of spherical NPs of the same diameter separated by 5 nm, respectively. (C) Spectra of the single spherical NP and the NP pair shown in A and B
- Figure 4. (a) Digital photo of handmade sugar and the compressible PDMS sponge. (b) Plan view SEM Image of PDMS sponge. The analysis of Au NPs by (c) TEM Image, (d) UV-Vis spectrum and DLS histogram, respectively.
- Figure 5. ATR-FTIR spectra of dielectric material (a). UV-Vis spectra for absorption test of PDMS sponge and PDA coated PDMS sponge (b). Digital photo (c) of PDMS sponge (i), PDMS sponge/PDA (ii), PDMS sponge/PDA/Au (iii-viii) and PDMS sponge/Au (ix). Cross section of SEM images of PDMS sponge/PDA/Au with dipping

time for 6 hours (d), 24 hours (e), 60 hours (f), respectively and PDMS sponge/Au (g).

Figure 6. (a) The schematic structure of TENG. Output performance of TENG with variation tribo-layer material: (b) Open circuit voltage (V_{oc}) and (c) Short circuit current (I_{sc}). (d) The cross section of the capacitance properties of TENG. (e) The schematic diagrams of the pores before and after compressed.

Figure 7. (a) The illustration attachment of Au NPs on PDMS with coating PDA and without coating PDA. Cross section of SEM images of Au NPs on PDMS (b) with coating PDA and (c) without coating PDA. The performance of TENG without gaps (d) Open circuit voltage (V_{oc}) and (e) Short circuit current (I_{sc}).

Figure 8. Output performance of TENG with increasing dipping time in Au NPs solution: (a) Open circuit voltage (V_{oc}) and (b) Short circuit current (I_{sc}). (c) The output voltage, current and power under different external loads. (d) Durability test of TENG. (e) Demonstration of turn on commercial LEDs.

Figure 9. Synthesis route of chain-like Au@TiO₂ structure.

Figure 10. The UV-Vis spectra of Au NPs aggregates formation under different experimental condition: (a) without and (c) with NaCl in ethanol, where the incubation time was 6 hours. TEM Images of Au NPs (b) isolated and (d) chain-like of Au NPs.

Figure 11. (a) The UV-Vis spectra of Au NPs (black color), isolated Au@TiO₂ (red color), and chain-like Au@TiO₂ (blue color) including digital photo of Au NPs (i), isolated Au@TiO₂ (ii), and chain-like Au@TiO₂ (iii), respectively. TEM Images and DLS histograms of (b-c) isolated and (c-d) chain-like of Au@TiO₂, respectively.

Figure 12. (a) The UV-Vis spectra of isolated Au@TiO₂ in ethanol (black color), in mixture 0 day (red color), and in mixture 6 day (blue color). Size distribution of isolated Au@TiO₂ in (b) ethanol, (c) mixture 1 day and (d) mixture 6 days. (e) TEM image of mixture isolated Au@TiO₂.

Figure 13. (a) The UV-Vis spectra of chain-like Au@TiO₂ in ethanol (black color), in mixture 0 day (red color), and in mixture 6 day (blue color). Size distribution of chain-like Au@TiO₂ in (b) ethanol, (c) mixture 1 day and (d) mixture 6 days. (e) TEM image of mixture chain-like Au@TiO₂.

Figure 14. The UV-Vis spectrum of Methylene Blue degradation using isolated Au@TiO₂ under (a) dark condition, (b) UV, (c) visible and (d) UV-visible illumination.

Figure 15. The UV-Vis spectrum of Methylene Blue degradation using chain-like Au@TiO₂ under (a) dark condition, (b) UV, (c) visible and (d) UV-visible illumination.

Figure 16. (a) Time-dependent absorbance values at 664 nm in the time course of MB photocatalytic decomposition from isolated (straight line) and chain-like (dash line) of Au@TiO₂ without (black color), UV (blue color), visible (red color) and UV-Visible (green color) light illumination, respectively. (b) The statistic histogram of photocatalytic's rate constant of isolated (blue color) and chain-like (red color) of Au@TiO₂.

Figure 17. (a) Schematic illustration of MB degradation over Au@TiO₂. (b) Photothermal of isolated (red color) and chain-like (blue color) of Au@TiO₂

Au Nanoparticle-Based Composites for Triboelectric Nanogenerator and Photocatalysis Applications

Merreta Noorenza Biutty

Department of Polymer Engineering

The Graduate School

Pukyong National University

Abstract

Gold nanoparticle has good properties and often used as supporting material in many studies. Their unique properties and multiple surface functionalities have great attention in the field of environment, energy and catalytic. In this regard, we use Au nanoparticle-based composites for triboelectric nanogenerator (TENG) and photocatalytic applications. For the triboelectric nanogenerator application, Au NPs improves the dielectric properties of TENG's active material. Au NPs-embedded porous PDMS composites have successfully enhanced the output performance of TENG. For the photocatalytic application, the combination of Au-semiconductor composites shows the enhancement of their photocatalytic activity. The modified chain-like Au NPs have been synthesized and combine with titanium. This structure has been demonstrated for the degradation of methylene blue.

Keywords: Au nanoparticle, PDMS, triboelectric nanogenerator, photocatalysis

금 나노입자 기반 복합체를 활용한 마찰전기 나노발전기 및 광촉매 연구

Merreta Noorenza Biutty

고분자공학공

대학원

부경대학교

요약

금 나노입자는 뛰어난 특성을 가지고 있기 때문에, 많은 연구에서 지지체로 많이 사용됩니다. 그 독특한 특성과 여러 표면 기능은 환경, 에너지, 촉매 분야에서 큰 주목을 받고 있습니다. 이러한 점에서, 금 나노입자를 기반으로 한 복합체를 마찰전기 나노발전기(TENG)와 광촉매에 적용하였습니다. 금 나노입자를 TENG에 적용하면, TENG의 유전 특성을 향상시킬 수 있습니다. 금 나노입자를 포함한 다공성 PDMS 복합체는 TENG의 출력 성능을 증대시켰습니다. 광촉매로 사용한 경우에는, 금 나노입자와 반도체의 복합재료를 통해 광촉매 특성을 향상시켰습니다. 또한, 사슬과 같은 구조로 개질된 금 나노입자는 타이타늄과 결합하여 합성하였으며, 이 구조는 메틸렌 블루의 분해를 보여주었습니다.

키워드 : 금 나노입자, PDMS, 마찰전기 나노발전기, 광촉매

Chapter I. Introduction

I-1. Harvesting Energy

Harvesting energy significant growth due to a great desire to create portable and wireless electronic. Because of their limited lifespan, leaking out and replacement periodically, the use of batteries still to be huge environmental issues. Therefore, energy scavenging devices are designed to utilize energy around us then convert to electrical energy. A number of sources of energy harvesting have been used, such as solar energy, electromagnetic energy, thermal energy and kinetic energy. The various energy harvesting technologies were listed in Table 1 [1].

Table 1. Comparison of various energy harvesting technologies.

Energy Sources	Conversion Efficiency	Harvested Power	Technologies/Device
Solar energy	10-24%	Indoor: $10 \mu\text{W} / \text{cm}^2$ Outdoor: $10 \text{mW} / \text{cm}^2$	Photovoltaic generator
Radio frequency energy	50%	$0.1 \mu\text{W} / \text{cm}^2$	Radio frequency generator
Thermal energy	3%	$1\text{-}10 \text{mW} / \text{cm}^2$	Thermoelectric and pyroelectric nanogenerator
Mechanical energy	Source dependant	$100 \mu\text{W} / \text{cm}^2$	Electromagnetic generator, piezoelectric nanogenerator, and triboelectric nanogenerator

I-2. Triboelectric Nanogenerator (TENG)

Fundamentally, triboelectric nanogenerator utilizes the principle of triboelectric effect which the phenomenon of material becomes electrically charge after contact with different material through friction [2]. Hence, the surface charge on the material moves to equalize their electrochemical potential. When separated, the material has the tendency to keep or give the electron depending on the affinity of material. Consequently, the triboelectric charge was created on the surface.

I-2.1 Vertical-contact separation of TENG

There are four modes of TENG, such as (1) vertical contact-separation mode, (2) lateral sliding mode, (3) single electrode mode and (4) freestanding triboelectric-layer mode [2]. Since the device in this thesis applies the vertical contact-separation mode, the discussion will be focus only on this type of work mechanism. The simple contact-separation mode of TENG was shown in Figure 1. The TENG consist of two dielectric material that complete with the top and bottom electrodes on the stacked structure. For instance, physical contact between two dissimilar dielectric materials creates an oppositely charged surface. When they are separated by a distance (gap), the potential drop was created. If the electrodes are electrically connected by a load, free-electron will move from one electrode to another electrode. So it produces the opposite potential due to balancing the electrostatic field. Once the gap closed, the triboelectric potential charge-created potential disappears and the electron flow back [3].

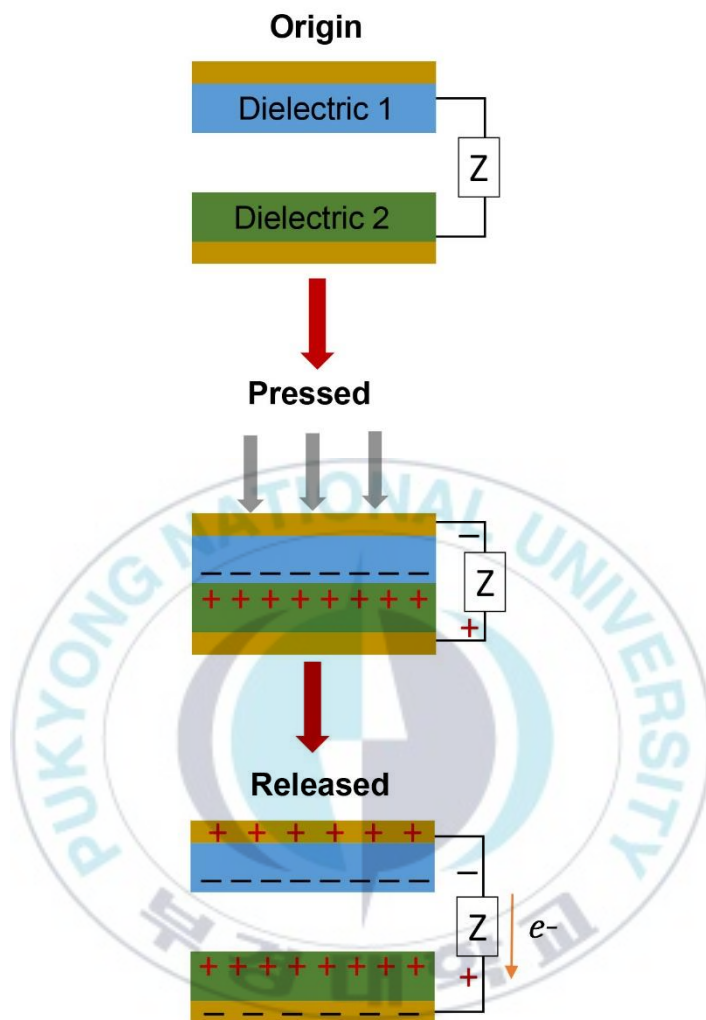


Figure 1. Simple mechanism of vertical contact-separation of TENG.

I-2.2 Improving of Triboelectric Nanogenerator Performance

The performances of TENG are depend on their principle works, which are the process of coupling contact electrification and electrostatic induction. The electrostatic induction can be explained by redistribution of electron in electrodes due to the influence of triboelectric charge. Therefore, the strategy to enhance performance of TENG is optimizing contact electrification and maximization of the surface triboelectric charge density. For the purpose, there are three ways to increase the surface charge density, such as (1) material selection, (2) surface physical modification and (3) surface chemical modification [4].

I-2.2.1 Material Selection

The key point for choosing material as a dielectric layer of TENG is consideration of the magnitude of electron affinity of material. For instance, the large difference in electron affinity of pair triboelectric layer results in the greater performance of TENG. In Table 2, the triboelectric series was presented which tested by Bill Lee (© 2009 by AlphaLab, Inc). The list of material that has tendency gaining electron (electronegative) or losing electron (electropositive) can be used as guidance for material selection in TENG design [4].

Table 2. Triboelectric series

Material	Charge Affinity (nC/J)	Material	Charge Affinity (nC/J)
Polyurethane foam	+60	Sorbothane	+58
Hair, oily skin	+45	Polyurethane solid	+40
Magnesium fluoride	+35	Nylon	+30
Machine oil	+29	Nylatron	+28
Glass	+25	Paper	+10
Wood	+7	Cotton	+5
Nitrile rubber	+3	Wool	0
Polycarbonate	-5	Acrylic	-10
Epoxy	-32	Styrene-butadiene rubber	-35
PET (mylar) solid	-40	EVA rubber	-55
Gum rubber	-60	Polystyrene	-70
Polyimide	-70	Silicones	-72
Vinyl: flexible	-75	LDPE	-90
Polypropylene	-90	HDPE	-90
Cellulose nitrate	-93	UHMWPE	-95
Polychloroprene	-98	PVC (rigid vinyl)	-100
Latex (natural)	-105	Viton, filled	-117
Epichlorohydrin rubber	-118	Santoprene rubber	-120
Hypalon rubber, filled	-130	Butyl rubber, filled	-135
EPDM rubber, filled	-140	PTFE (Teflon)	-190

I-2.2.2 Surface Physical Modification

Providing effectively contact in the performance of TENG, the material can be modified by physical modification. As a result, the increasing contact area can produce higher surface charge density. Moreover, surface modification can give nanoscale roughness contributing more triboelectric charges during the friction process. In addition, creating porous structure in dielectric material also presents

more surface area. The patterned of PDMS thin film with line feature, cubic features, pyramid features; coated polymer nanowire; and nanopores on aluminium electrode have been demonstrated to give a better performance [5-7].

I-2.2.3 Surface Chemical Modification

Not only physical modification, but also chemical modification become one way to enhance the performance of TENG. Modified proper functional group in the surface is a critical basic approach to boost output electricity. Some chemical modification have been demonstrated. For example, Shin et al presented the plasma-treated PET was functionalized with poly-L-lysine or FOTs [8]. They also introduced positively charge amino group ($-NH_3$) and negatively charged $-CF_3$ groups. In addition, Li et al also presented an effective surface modification a PET film via ICP etching using carbon tetrafluoride (CF_4) and Oxygen (O_2) gases [9]. Both of them showed the drastic enhancement performance of TENG.

I-3. Mussel-Inspired Polydopamine Coating

Many efforts to get a good method for surface chemical modification play an important role in recent technologies. Nowadays, the invention of inspired-method by the adhesive protein from mussels for attachment to wet surface have been trend in chemical field [10-12]. In nature, mussels are the one of fouling organism that can attach to all types of inorganic and organic surface [13]. The chemical substance in this organism, especially 3,3-dihydroxyl-L-phenylalanine (dopamine) and lysine

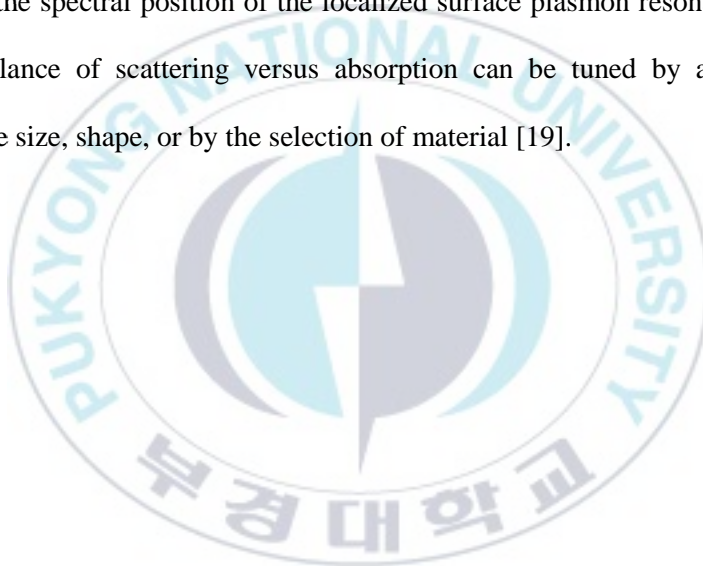
amino acids, is the key to their strong adhesive property. Therefore, dopamine and other catechol groups known as a binding agent. The process of this coating method is favorable due to the simple way in which a simple immersion of the substrate in the aqueous polydopamine (PDA) solution. The important thing is imitated of the marine environment with adjusting alkalinity conditions at pH 8.5. Using this condition, the dopamine can self-polymerize then spontaneous deposition of a thin polymer film. Recently, Bielawski proposed molecular mechanism that PDA is a supramolecular aggregates of monomer that were held together via a combination of charge transfer, π -stacking, and hydrogen bonding interactions [14]. Interestingly, the polydopamine coating is able in various materials such as, noble metal (Au, Ag, Pd and Pt), metal-oxide, oxides, semiconductor, ceramics, synthetic polymer (PET, PTFE, PDMS, and PUUK) [15].

I-4. Metal Nanoparticles

The particle having size of 1 – 100 nm was called nanoparticles. Due to their small size, nanoparticles have unique properties compared to bulk material. In the case of metal nanoparticles, their optical properties have long been of concern in the field of physical chemistry. The extinction, absorption, and scattering are the primary properties of interest. It to be noted that the electrodynamics of metal nanoparticle very depends on their size and shape [16-17].

I-4.1 Localized Surface Plasmon Resonance

Localized surface plasmon resonance (LSPR) refers to the collective oscillation of free electron at the interface of metallic structures, with could be produced through the electron-magnetic interaction of the metal with incident light of a specific wavelength [18]. This process was shown in Figure 2. The LSPR of metal NPs is strongly dependent on the dielectric constant of the metal ant the surrounding material. Therefore, the spectral position of the localized surface plasmon resonance (LSPR) and the balance of scattering versus absorption can be tuned by adjusting the nanoparticle size, shape, or by the selection of material [19].



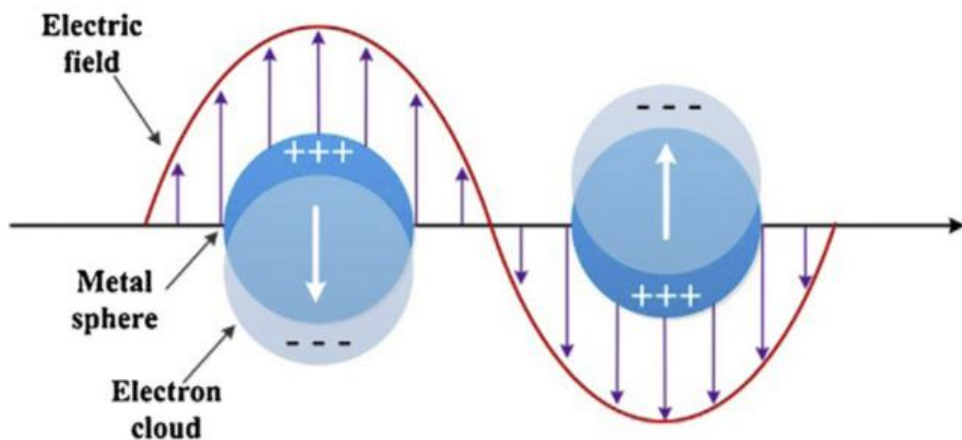
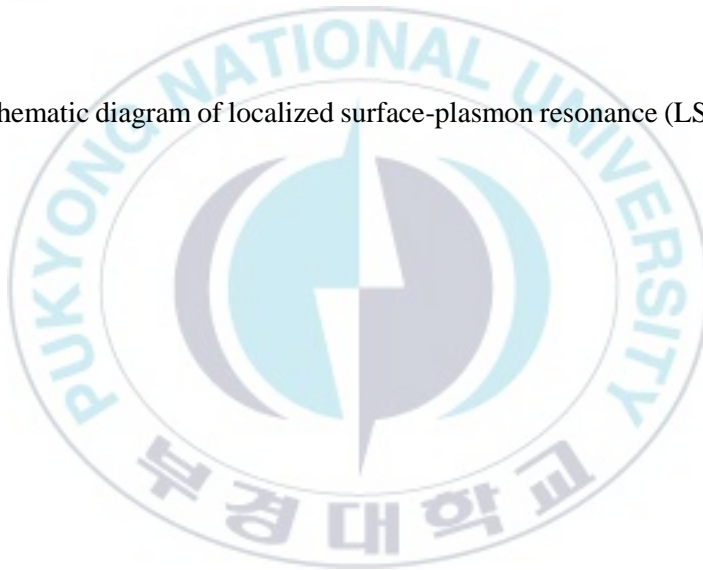


Figure 2. Schematic diagram of localized surface-plasmon resonance (LSPR) process.



I-4.2 Plasmonic coupling

The plasmonic coupling occurred when two or more plasmon nanoparticle is in close vicinity and consequently the localized of the individual nanoparticle interact with each other via their optical near field, creating a couple of LSPR modes [20]. Upon the plasmon coupling process, the resonance of single-particle start to hybridize, and their resonance spectra peak wavelength will redshift. In figure 3, the “hot spot” in the coupled-nanoparticle was clearly shown. In this condition, the interparticle distance and configuration can affect the resonant frequencies of a couple of nanoparticles. A narrow band was shown in a single nanoparticle. However, the large redshift spectra were exhibited when the gap between the two nanoparticles is closer (coupled).

In the case of photocatalysis, the near field coupling extracts the energy from the dipole radiation and reduces the radioactive scattering. It was useful for nanospheres the whole scattering it otherwise significant. Moreover, the enhanced electric field extends beyond the surface region on a single nanoparticle [21]. In addition, the strong coupling interface within nanoparticle can enhance the photogenerated charge separation transfer. Therefore, it can enhance the photocatalytic reaction.

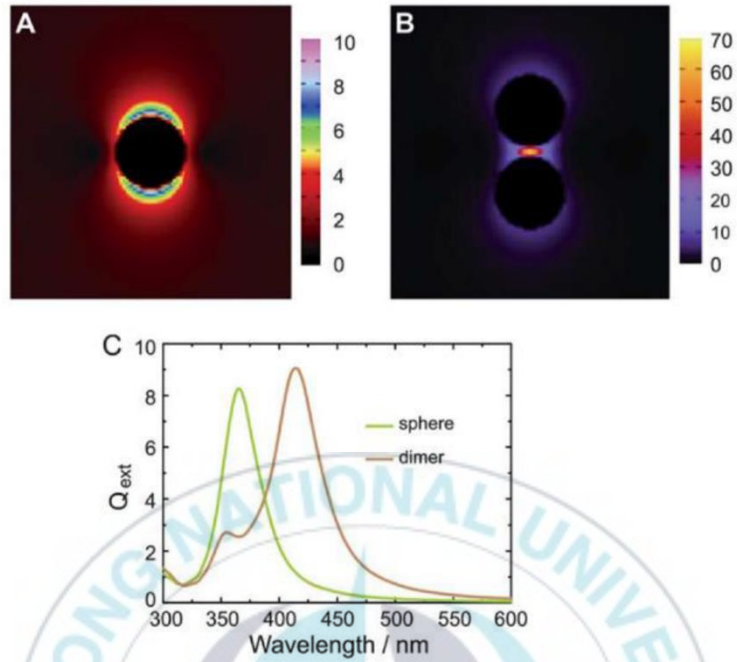


Figure 3. Plasmonic coupling (A, B) Near field enhancement distribution produced by a silver spherical NP with $D = 25$ nm and by a pair of spherical NPs of the same diameter separated by 5 nm, respectively. (C) Spectra of the single spherical NP and the NP pair shown in A and B [21].

I-5. Photocatalysis

I-5.1 Semiconductor Photocatalysis

In general, photocatalysis uses the semiconductor to absorb photons then create active electron and holes. This process can initiate the reduction or oxidation of chemicals. Semiconductors have a relatively small bandgap, and they are not conductive as their valence band is filled with electrons and so the electrons are not mobile within the material. In the presence of external energy source electrons can be excited to the conduction band which was previously empty, thereby provides partial conductivity of the semiconductor. However, the low photocatalytic efficiency and the poor absorb of visible-light become major issues in this field [22]. The former is due to the recombination of excited electron and holes. Therefore, extensive research on heterogeneous photocatalytic has been conducted for a few decades.

I-5.2 Metal-Semiconductor Photocatalysis

Hetero-structure photocatalytic recently come into focus as a promising technology for high-performance photocatalysis, especially for the case of a metal-semiconductor combination. Compare to semiconductor photocatalysis, metal-semiconductor photocatalysis gives two distinct features, which are Schottky junction and LSPR [21]. For instance, the Schottky junction results from the contact of the noble metal and the semiconductor. It provides to prevent electron and hole from passing through them. Moreover, upon process, metal acts as a charge-trap center to host more active sites

for photoreaction. While, the LSPR from metal brings several benefits, such as to enhance the visible light absorption, create a local electric field, local heating effect, and reduce electron-hole diffusion length [23-25]. In addition, generally metal-semiconductor can excite charge carriers in semiconductors through plasmon-induced resonance energy transfer and hot electron injections process. However, in this regard, only hot electron injection will be discussed.

I-5.3 Hot-Electron Injection

After light absorption in the nanostructures and LSPR excitation, plasmons can decay, transferring the accumulated energy to electrons in the conduction band of the material. This process produces highly energetic electrons, also known as 'hot electrons', which can escape from the plasmonic nanostructures and be collected by, for example, putting the plasmonic nanostructures in contact with a semiconductor, thereby forming a metal-semiconductor Schottky junction [26-27]. In detail, for the case of photocatalysis, hot electrons with energies higher than the Schottky barrier energy can be injected into the semiconductor with an emission efficiency dependant on their energy [28]. The energy needed for hot electrons to overcome the energy barrier in this system is considerably smaller than the bandgap of the semiconductor. After the injection of hot electrons into the neighboring semiconductor, the plasmonic nanostructures are left positively charged because of electron depletion. Recent studies have shown that their efficiency rises slightly with increasing temperature because of a higher probability of hot-electron injection [29]

Chapter II. Au Nanoparticles-embedded Porous PDMS Composites for Triboelectric Nanogenerator with Enhanced Performance

II-1. Introduction

Imposing research efforts have been intensively developed for sustaining the massive world's energy consumption. A huge energy reservoir from environments such as the wind, the sun and biomass, has been proven that can be potentially utilized to solve energy crisis problem [29]. Due to low cost, lightweight, simple and efficient technique, the triboelectric nanogenerator (TENG) becomes an important role in the field of promising alternative energy by scavenging mechanical energy [2,30]. Therefore, the enhancements of TENG performance have attracted great attention for various applications, such as self-powered active sensors [32-33], self-electroplating [34] micro-scale power source [35-38] and mega-scale power source [39-42].

The fundamental work of TENG was adopted from a common phenomenon in people's life, called the triboelectrification effect [2]. It termed as contact electrification, it is considered as generating an electrostatic charge by physical contact between two materials that have different polarities, different electron affinity, and different triboelectric ability [43]. Hence, the selection of triboelectric material

must be considered. Generally, the fabrication of TENG consists of a negative side using the material which has a more electronegative group [44] and a positive side using low work function material [45]. Both of them should be separated from each other. In concern, researchers as efforts in improving the output performance of TENG have demonstrated material modification and surface functionalization [46-49].

Considering the requirement of flexibility, compressibility, durability and economic efficiency for TENG, combining metal and polymer are offered as competitive material to achieve great performance. Recently, various types of nanoparticle (NPs) are used to improve surface charge by increasing the friction when the external load applying in contact with two material [48-51]. Furthermore, a highly compressible material, especially sponge-structure has been reported in order to increase the contact area [47, 48, 51, 52]. However, so far, there is still no reported that compares the effect between physical and chemical techniques in the modification of material in order to enhance the output performance of TENG, particularly in sponge-structured based. In this regard, modification of sponge polydimethylsiloxane (PDMS) with polydopamine (PDA) and gold nanoparticle (Au NPs) have been designed as an effective dielectric. By using sugar templates, the flexible sponge-structured PDMS has been successfully fabricated. Furthermore, a facile path for surface modification in which self-polymerization of dopamine through a simple dip-coating method has been applied in this work. In the presence of catechol and N-H groups, Au NPs can chemically be attached to the pore of PDMS sponge. For comparison, an-modified of

sponge PDMS was combined also with Au NPs by simple dipping in Au NPs solution without rinse DI water. Due to the micro-size of the pore, the Au NPs can be entrapped in the bottom of pore sponge PDMS with this method [48]. The higher performance TENG was showed in sponge PDMS/PDA/Au, compare to sponge PDMS/Au. The optimum effective dielectric material of TENG can achieve electricity corresponds with voltage and current about 180 V and 1.9 μ A, respectively. This prototype has been applied to operate the commercial LED.

II-2. Experimental Section

II-2.1. Material

Poly(dimethylsiloxane) SYLGARD 184 Silicone Elastomer base and the thermal curing agent were obtained from Dow Chemical Company. Dopamine hydrochloride (98%), Gold (III) chloride trihydrate (99.9%) and sodium citrate tribasic dihydrate (99.0%) were purchased from Sigma-Aldrich. All the chemicals were used as received.

II-2.2. Procedure

II-2.2.1. Fabrication of PDMS sponge

The commercial sugar was kneaded by adding DI water and then cast onto a specific size (3 cm \times 2 cm \times 1 cm) of sugar mold. Afterward, the sugar template was peeled away from the mold. The mixture of PDMS base and the curing agent was poured in

a ratio of 10:1 by weight on a petri dish. Two sugar templates were placed into a petri dish containing 3 grams (total weight) mixture of PDMS. Moreover, the petri dish was degassed in a vacuum oven at room temperature for 4 hours. By capillary forces, the PDMS mixture can infiltrate into the sugar templates. The absorbed PDMS in sugar templates were cured at 80°C for 2 hours. Thereafter, the sugar templates were dissolved using DI water for several times following by washing for overnight. Therefore, the sugar was removed from the PDMS sponges. Then, the PDMS sponges were dried at ambient temperature for a day. While, the PDMS film was made using the same mixture solution. However, before the curing process, the mixture was degassed using a vacuum oven for 10 minutes to remove the bubble.

II-2.2.2. Synthesis of Gold Nanoparticle

Au NPs were synthesized by the citrate reduction method. Briefly, a 500 mL aqueous solution of HAuCl₄ (0.1 g) was heated until boiling, and 25 mL of sodium citrate solution (0.5 g in 25 mL) was added to the boiling solution. The mixture was further boiled for 15 min with vigorous stirring and then cooled to room temperature. The excess of citrate was eliminated by centrifugation at 9000 rpm for 40 minutes and re-dispersed in DI water.

II-2.2.3. Modification of PDMS Sponge

The PDMS sponge was surface-modified by immersing in dopamine solution and gold nanoparticle, in sequence. The dopamine solution was prepared by dissolving

dopamine in 10 mM Tris buffer pH 8.5. Then, the sponge was immersed in dopamine solution (2 mg/mL) for 4 hours. After PDA coating, the sponges were washed using DI water for overnight. Hereafter, PDA-coated PDMS sponge was immersed in 20 mL Au NPs solution for 6 – 60 hours.

II-2.2.4. Fabrication of TENG

The modified PDMS sponge/PDA/Au will be used as a dielectric layer. Before using, the dielectric material was washed using DI water and was dried slowly for 2 days in room temperature to remove water. The TENG has two separation components, the bottom part, and the top part. The bottom part consisted of an acrylic substrate, with dimensions of 5 cm × 5 cm × 0.5 cm. The PDMS sponge/PDA/Au (3 cm × 2 cm × 0.5 cm) was produced on the copper electrode attached by the double side Kapton tape. The top part consisted of another acrylic substrate, in which there was only copper electrode. The bottom part and top part were separated by four springs. Finally, lead wire connected to each of the electrodes for conducting measurement.

II-2.3. Measurement

UV–Vis spectra were obtained on an Agilent Carry 8454 UV-Visible spectrophotometer. Particle size distribution was evaluated by dynamic light scattering (DLS) using a Malvern Zetasizer Nano ZS90. Transmission electron microscopy (TEM) was carried out with the Hitachi H-7500 instrument operating at 80 kV. Samples for TEM were prepared by drying a drop of Au NPs solution onto a

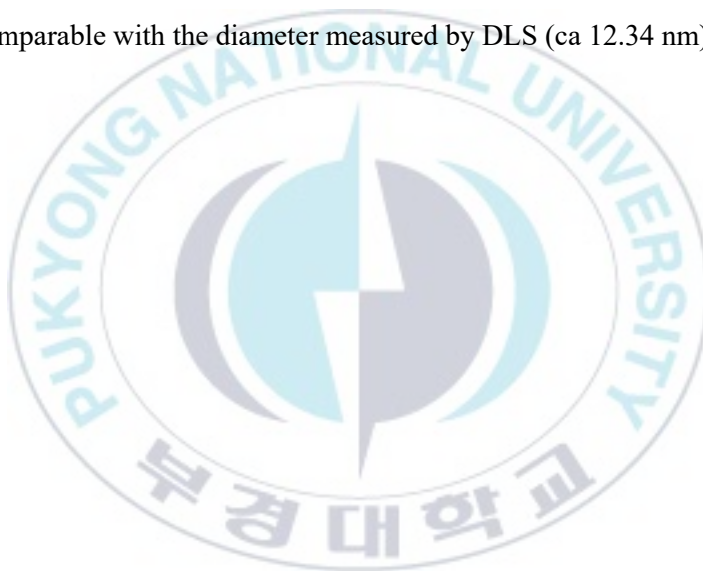
carbon-coated copper grid at room temperature. Attenuated Total Reflectance Fourier Transform Infrared (ATR-FTIR) spectra were obtained by using a JASCO FT/IR-4100 spectrometer. All FTIR measurements were performed on freshly prepared samples. The structure section of the sponge was analyzed by Field Emission Scanning Electron Microscopy (FE-SEM). To measure the output performance of TENG, 2 kg of weight-balanced was used to simulate the press-release process. The pressure was controlled using stopper 3mm (l/o). The short circuit current and open-circuit voltage of TENG was measured using a Keithley 6514.

II-3. Results and Discussion

II-3.1. Characteristic of PDMS sponge and Gold Nanoparticle

The process of fabricating the dielectric tribo-layer PDMS sponge/PDA/Au is described. Simply, the dip-coating method was used for coating polydopamine and gold nanoparticles onto PDMS sponge. The hand-made sugar template from commercial sugar powder was used to make a replica of the flexible PDMS sponge (Figure 4a). In the production of PDMS sponge, it is notable that the sugar-templating process is one of fast production that only needs a few hours in the process. Moreover, it has a big potential for large-scale production that can be readily implemented [53]. The particle of sugar was used as the pore-creating agent. So, the porous sponge-like PDMS could be fabricated, as shown in Figure 4a, which has great compressibility but nontransparent. Scanning Electron Microscopy (SEM) in the Figure 4b exhibits

that the PDMS sponge carries open-network of the pore. It proves the PDMS entirely fills the sugar mold. Thereafter, we will introduce the PDMS sponge with gold Au NPs. As shown in the transmission electron microscopy (TEM) image (Figure 4c), we synthesized the well-separated spherical of Au NPs morphology has an average diameter of 12 nm by using the citrate reduction method. Au NPs solution has a narrow extinction at 520 nm (Figure 4d) which is attributed to the surface plasmon resonance (SPR) band of a mono-dispersed nanoparticle. In figure 4d, the diameter size was comparable with the diameter measured by DLS (ca 12.34 nm).



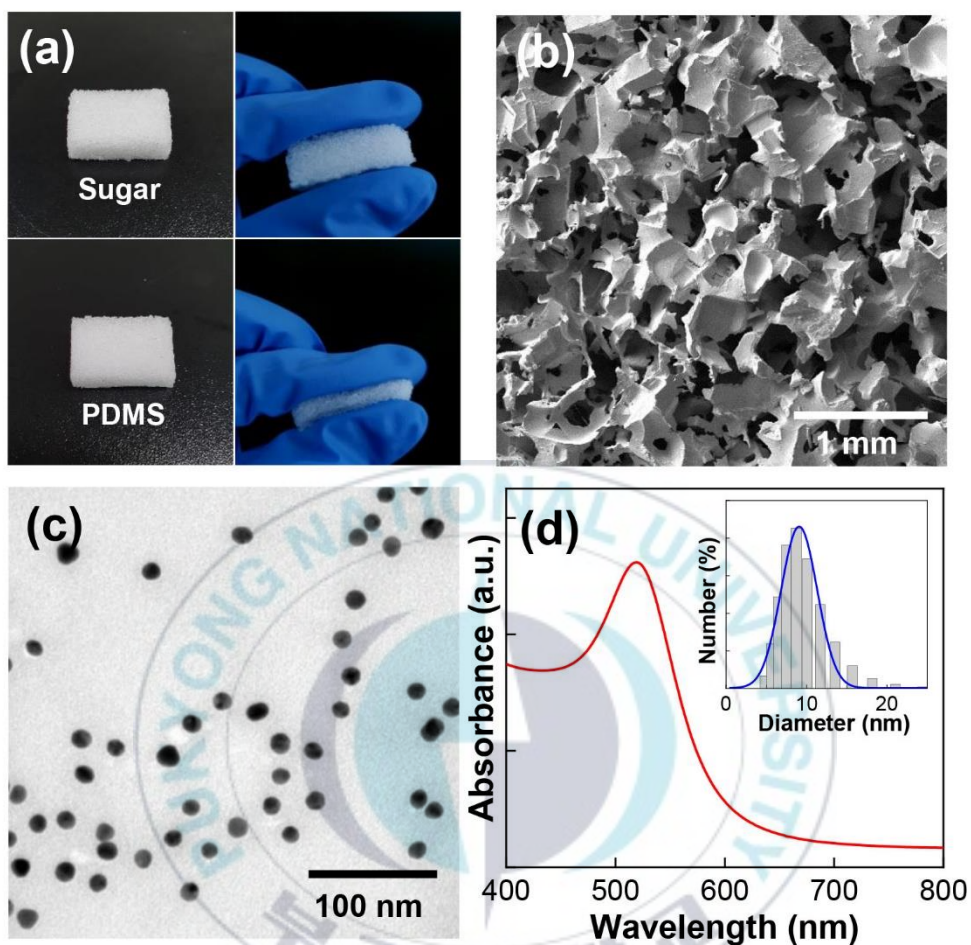


Figure 4. (a) Digital photo of handmade sugar and the compressible PDMS sponge. (b) Plan view SEM image of PDMS sponge. The analysis of Au NPs by (c) TEM image, (d) UV-Vis spectrum and DLS histogram, respectively.

II-3.2. Characteristic PDMS Sponge/PDA/Au

Polydopamine coating was used as an intermediate step in our system. As a binding agent, dopamine can be spontaneously polymerized into polydopamine under pH typical of marine environments conditions [15]. The PDMS sponges dipped in buffered dopamine at pH 8.5. In this case, controlling pH at alkaline conditions can initiate self-polymerization of dopamine. The PDA coated-PDMS sponge then washed by DI water several times to remove an-attached dopamine. Hereafter, the sponge was dipped in Au NPs water solution. The ATR-FTIR measurement regarding the binding interaction between PDMS sponge with PDA and Au NPs was investigated and discussed in the following (Figure 5a). The dopamine powder has observed for the initial reference of PDA-coated. The absorption band around 1260, 1010 and 792 cm^{-1} denoted stretching of Si-CH₃, Si-O-Si, (Si-(CH₃)₂) groups, respectively and 1407 cm^{-1} asymmetric C-H bending, which corresponds for PDMS [54, 55]. The transformations around 1510 and 1620 cm^{-1} denoted the stretching of C=C and bending of N-H groups, which specific for PDA [56].

The absorption test of Au NPs using UV-Vis spectroscopy has been analyzed. In Figure 5b, the spectra show decreasing absorbance of Au NPs corresponds to the concentration of nanoparticle. The modified PDMS sponge gives the better ability of absorption of Au NPs compare to an-modified PDMS sponge. It verifies that modified sponge PDMS using polydopamine could improve the attachment of Au NPs on their surface. Moreover, this also shows that the increasing of the dipping

time in Au NPs can increase the number of Au NPs in/on sponge, which indicated by discoloration. In Figure 5c, the color of PDMS sponge changes from white (i) to brown after 4h dipping in polydopamine solution (ii). Then, the color of PDMS sponge/PDA becomes darker after dipping in Au NPs solution (iii-viii). While, the color of an-modified PDMS sponge-embedded Au NPs was light purple (ix). This absorption test was comparable to FE-SEM analyzed. The morphology of tribo-layer was observed by FE-SEM (Figure 5d-g). The Au NPs clearly showed on the surface of PDMS sponge which was modified with polydopamine (Figure 5d-f). Otherwise, the density of gold nanoparticle was observed with the increasing of dipping time. Moreover, filling Au NPs in the pore of PDMS sponge with and without the presence of polydopamine has been compared. As shown in Figure 5g, only a small amount of Au NPs appears on the surface of the sponge. Without PDA-coated, slowly drying made the Au NPs only deposited on the bottom side of pores.

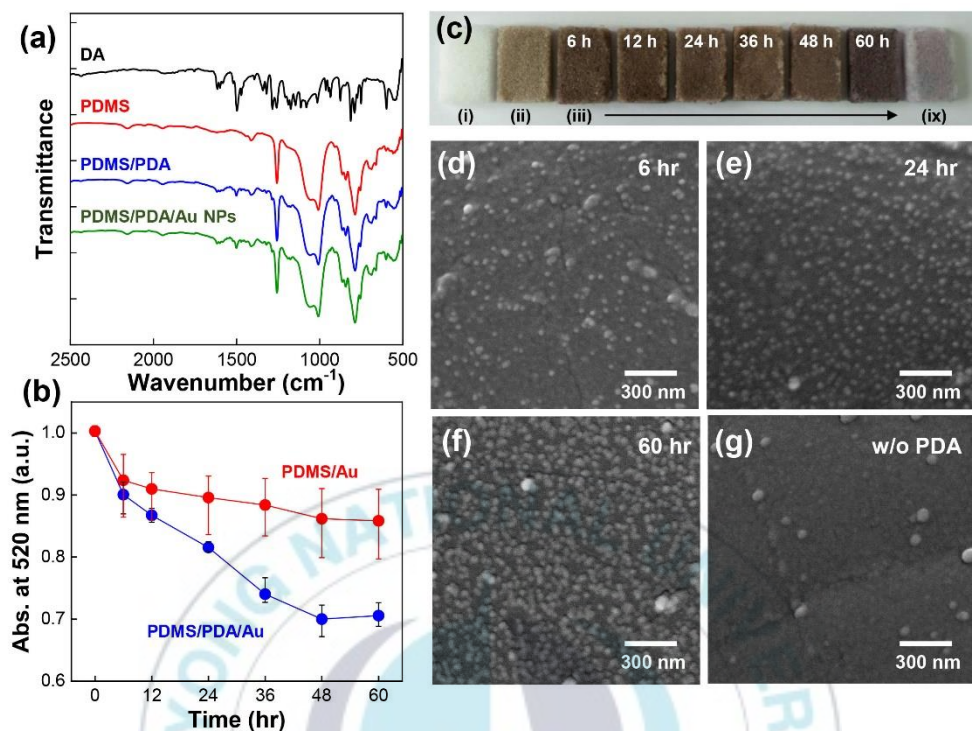


Figure 5. ATR-FTIR spectra of dielectric material (a). UV-Vis spectra for absorption test of PDMS sponge and PDA coated PDMS sponge (b). Digital photo (c) of PDMS sponge (i), PDMS sponge/PDA (ii), PDMS sponge/PDA/Au (iii-viii) and PDMS sponge/Au (ix). Cross section of SEM images of PDMS sponge/PDA/Au with dipping time for 6 hours (d), 24 hours (e), 60 hours (f), respectively and PDMS sponge/Au (g).

II-3.3. Comparison Performance of Triboelectric Nanogenerator

As shown in figure 6a, the fabrication of TENG consisted of a dielectric layer, top and bottom electrode. Both the electrodes were made of copper foil, and were each fixed on acrylic plate using Kapton film. Thereafter, for the bottom side, a Kapton tape was glued onto the side of the dielectric layer. While, the other side consisted of only electrode of copper. Further, the spacers for supporting contact and separation made by four springs that fixed on the corner of acrylics square plates which give the gap around 3 mm between the bottom and the top part.

The output voltage of TENG was measured under open-circuit condition. On original state, without press-release activity, there is no charge transfer. However, when the external force was applied, the friction between PDMS and Au generate the difference potential. The positive and negative charges resulted on the surface. Since, the electron transfer from Au NPs to the PDMS sponge. While, the current was measured under short-circuit condition. The PDMS sponge has negative charge, which can induce the positive charge for one of electrode. The positive charge from Au NPs also induce negative charge in the other electrode. Using external circuit, the electrons flow from the electrode to another electrode. The current was generated when the electrostatic equilibrium have been reached.

For investigating the effect of modification PDMS sponge, the output performance correspond with open circuit voltage (V_{oc}) and short circuit current (I_{sc}) were summarized in Figure 6b and 6c. First, the comparison of PDMS film and PDMS

sponge were analyzed to describe the effect of pore structure in performance of TENG. The pores in sponge-like structure of PDMS play an important role in determining output performance of TENG. The result showed that it obtain a higher output performance in sponge PDMS, compare with the flat film of PDMS. In this case, the pore-form can increase the surface area of material. Therefore, the surface charge during the contact-separation process also increase. Moreover, from the V-Q-x relationship for contact mode TENG [32], the output voltage can be expressed by

$$V = \frac{(\sigma_0 - \Delta\sigma) \cdot x(t)}{\epsilon_0} - \frac{\Delta\sigma \cdot d_1}{\epsilon_0 \epsilon_r} \quad (1)$$

Where $\sigma_0, \Delta\sigma, \epsilon_0, \epsilon_r$ are triboelectric charge density of PDMS, transferred charge on the electrode, vacuum permittivity and relative permittivity of PDMS, respectively. Then, $x(t), d_1$, and t are distance of interlayer between top part and bottom part, thickness of material (PDMS) and time, respectively. The above electric properties was describe on Figure 6d.

In detail, when the device work on open circuit condition, the value $\Delta\sigma$ was zero (no charge transfer). So the V_{oc} can be determined by

$$V_{oc} = \frac{\sigma_0 \cdot x(t)}{\epsilon_0} \quad (2)$$

From this equation, there is no correlation between voltage and the dielectric material. However, contact-mode TENG can be used as energy storage and energy output. Consequently, the capacitance become important properties in this performance.

Furthermore, the value of σ_0 is dependent on the capacitance of generator. So that, we can obtain the maximum capacitance (C_{max}) by

$$C_{max} = \epsilon_0 A \cdot \frac{\epsilon_r}{d_1} \quad (3)$$

The surface charge density is proportional to capacitance. In summary, using this understanding, the output performance of TENG can be correlated to dielectric material properties, especially for permittivity and the thickness of material. The optimize of output performance of TENG can be adjusted by controlling the ratio of ϵ/d . In this study, initial thickness of PDMS sponge and PDMS flat film were same (5mm). However, when the external force was applied, the thickness of PDMS sponge was shrink, as shown in Figure 6e. According to equation 3, the output performance of TENG increase with a decrease of the thickness of material. Therefore, pore formed in PDMS, not only can increase the surface area but also can effectively reduce the thickness of PDMS.

In order to study about the effect of gold nanoparticle, PDMS sponge with (PDMS sponge/Au NPs) and without Au NPs have been compared. The result shows that, in the presence of Au NPs, the TENG can generate higher value of V_{oc} and I_{sc} . The metal nanoparticle has good properties due to enhance the performance of TENG. Au NPs has tendency to lost electron, while the PDMS has tendency to gain electron. The different affinity of these two materials can enhance the performance of triboelectric. Moreover, the relative permittivity of the Au NPs (6.0) is higher than PDMS (3.0).

From the Lichtenecker logarithmic mixture formula [57], a new value of dielectric constant of filling particles having irregular geometry and randomly distributed can be determined. For simply, filling higher dielectric particle (Au NPs), the permittivity of material (PDMS/Au NPs) in TENG can increase. Therefore the output performance of TENG was enhanced.

In addition, the PDA coating method before attaching Au NPs on the surface of PDMS sponge have been demonstrated. Compared with only PDMS sponge, PDA coated-PDMS sponge has the higher performance, even though the performance still lower than PDMS sponge/Au. Polydopamine has catechol and amine groups which has function as a basis for the strong adhesion. The coating of PDA can strengthen the interfacial polarization of the PDMS sponge by appearing strong dipoles from –NH and –OH around coated surface. Consequently, the polarization of material can increase the dielectric constant. It is worthwhile to note that Wang et al have been recently study about improvement energy storage from dielectric polymer with polydopamine [58]. Otherwise, the amine groups is the most triboelectrically-positive functional groups. So, it can creates largest enhancement for charge density generated.

Finally, the PDMS sponge in the presence of Au NPs for PDMS sponge with and without modified have been compared. Based on Figure 5b, the an-modified of PDMS sponge can absorb 0.77 nM of 12 nm Au NPs after 60h dipping in Au NPs solution. The concentration of Au NPs has identical amount with the modified PDMS

sponge which can attach 0.76 nM of 12 nm Au NPs after 12h dipping in Au NPs solution. In this case, using identical of the amount of Au NPs on the surface, the PDMS sponge/PDA/Au can enhance huge of V_{oc} and I_{sc} . From the illustration in Figure 7a, without coating process, the Au NPs were likely only deposited to the bottom of pore due to gravity force. Hence, the agglomerated of Au NPs were obtained. While, with coating process, the Au NPs tend to spread out in the surface of PDMS. So, the opportunity of material to rub was more effective. In this case, the distribution of Au NPs on the PDMS sponge can affect the performance of TENG. In order to know the distribution of Au NPs, the top view of scanning electron microscopy have been showed. The Figure 7b-c proved that with polydopamine coating (Figure 7b), the spreading distribution of Au was more homogeneous than an-coated PDMS (Figure 7c).

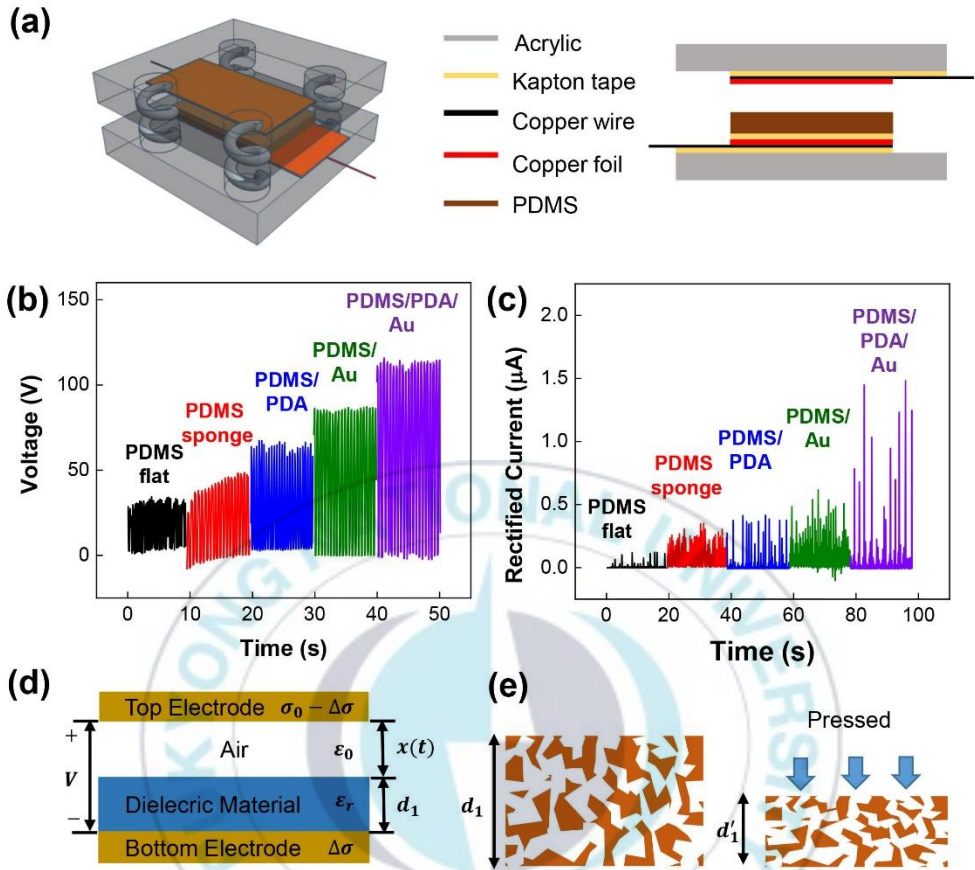


Figure 6. (a) The schematic structure of TENG. Output performance of TENG with variation tribo-layer material: (b) Open circuit voltage (V_{oc}) and (c) Short circuit current (I_{sc}). (d) The cross section of the capacitance properties of TENG. (e) The schematic diagrams of the pores before and after compressed.

II-3.4. Contribution Material Inside of Pore

The modification of PDMS sponge with polydopamine and gold nanoparticle was successfully enhance the output of TENG. However, the top surface of material dominantly contribute to generate surface charge in the vertical contact-separation method. In order to study the contribution of material inside the pore, the performance of TENG without gaps have been demonstrated in Figure 7d-e. According to eq. 2, the interlayer distance between top electrode and the top surface of material ($x(t)$) will effect the output voltage of TENG. The higher distance will produce the higher electricity, in the form of voltage. This is proven that without the gaps, the PDMS flat film could not produce the electricity, as shown in Figure 7d. However, for the PDMS sponge, the device still generate electricity even though the value is lower compare to PDMS with the presence of gaps. It shows that the pore can act as an airgap which facilitate the friction of material inside the pore. Moreover, the enhancement of PDMS sponge/PDA/Au still be performed without gaps. Therefore, it can be confirmed that the charge from material inside the pore can induce charge on the electrode. In summary, the friction of material inside the pores gives contribution in the performance of vertical contact-separation of TENG.

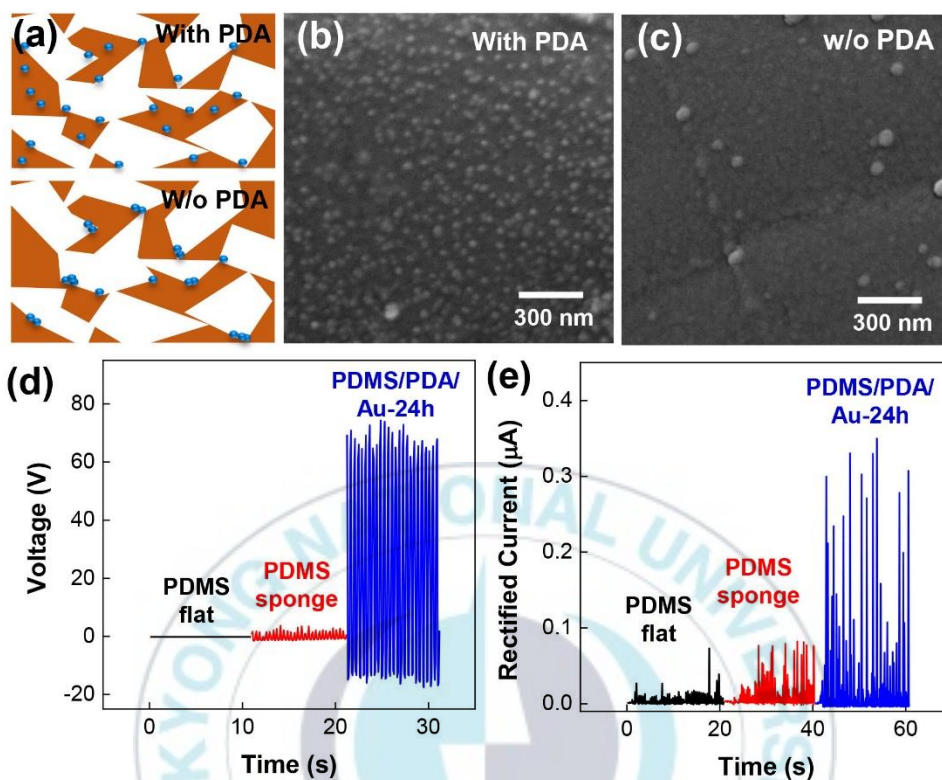


Figure 7. (a) The illustration attachment of Au NPs on PDMS with coating PDA and without coating PDA. Cross section of SEM images of Au NPs on PDMS (b) with coating PDA and (c) without coating PDA. The performance of TENG without gaps (d) Open circuit voltage (V_{oc}) and (e) Short circuit current (I_{sc}).

II-3.5. Optimum Condition of Triboelectric Nanogenerator Performance

As know before, the modified PDMS sponge has better ability to absorb Au NPs. Therefore, the dipping time PDMS sponge/PDA in Au NPs has been varied (6-60 hours) to investigate the effect of dipping duration in performance of TENG. The absorbance of gold solution decrease with increasing of the dipping time and accordingly the amount of Au NPs which attached on PDMS/PDA can adjust by controlling dipping time. As shown in Figure 8a and 8b, the performance of TENG enhance with increasing concentration of Au Nps. The TENG can achieved open circuit voltage of 180V and short circuit current of 1.9 μ A. However, after optimum condition, which is 24 h dipping time, the performance were weakened. The hush of Au NPs on the surface of PDMS sponge/PDA will decrease the contact-area and friction between Au NPs and PDMS sponge/PDA. The opportunity contact between same materials (Au with Au or PDMS sponge/PDA with PDMS sponge/PDA) will arise and consequently the effective friction area will decrease. Nevertheless, eventually the TENG modification of PDMS material can enhance 6 times higher compare to basic structure of PDMS (PDMS flat film). In the optimum condition, the power of TENG reaches a peak value of 5.1 μ W at a resistance of 7M Ω , as shown in Figure 8c. The durability of the device was demonstrated over 1500 cycles (Figure 8d), indicating good stability for long-term operation. Without using capacitor, the optimum TENG connected with 30 commercial LEDs as shown in Figure 8e.

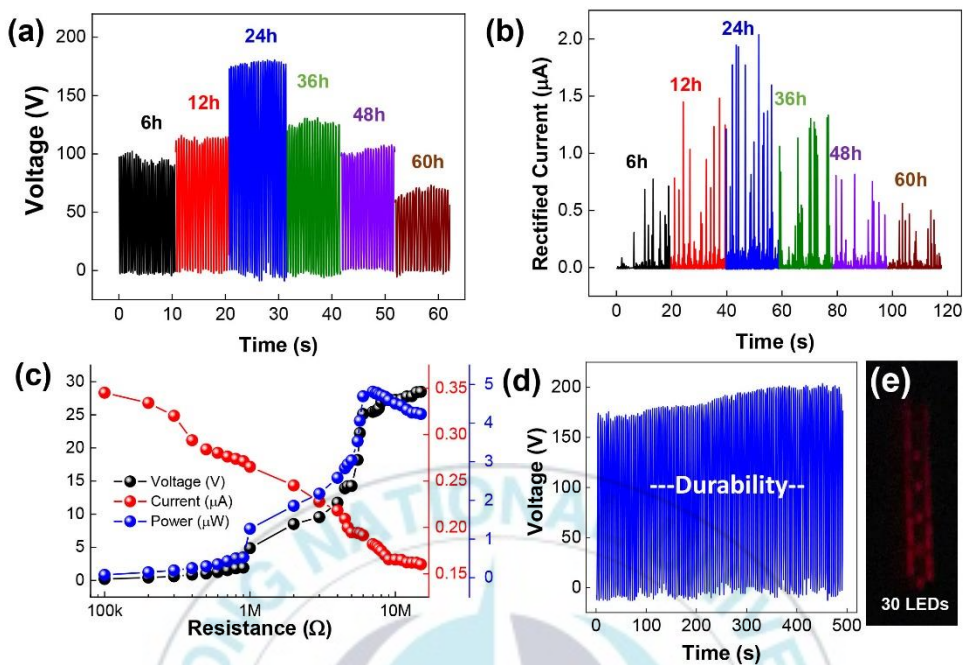


Figure 8. Output performance of TENG with increasing dipping time in Au NPs solution: (a) Open circuit voltage (V_{oc}) and (b) Short circuit current (I_{sc}). (c) The output voltage, current and power under different external loads. (d) Durability test of TENG. (e) Demonstration of turn on commercial LEDs.

II-4. Conclusion

In conclusion, we have demonstrated a simply method of embedded Au NPs in modified-PDMS sponge with polydopamine as dielectric material for enhancing the performance of TENG. The PDMS sponge has more flexible that also give pore to cover more effective friction area compare than PDMS flat film. The contribution of material inside the pores play a role in improvement TENG's performance. In addition, polydopamine coating has better ability to attach Au NPs and consequently enhance the V_{oc} and I_{sc} . Therefore, combination between physically surface and chemically surface can well enhance the performance of TENG. The nanogenerator with this material was succesfully demonstrated in application for lighting LEDs. This facile and scalable method provides a promising large-scale power generator.

Chapter III. Synthesis of Chainlike Au@TiO₂ and Their Photocatalytic Activity

III-1. Introduction

The semiconductor is common material in photocatalytic field due to their unique energy band structure. However, the large band gap and the favoring recombination of electron-hole pair, play a diminishing photocatalytic reaction [22]. In other hand, the metal nanoparticles have the great plasmonic optical properties which provide strong light absorption and scattering cross section [59, 60]. In addition, the localized surface plasmon resonance (LSPR)-induced give a strong local electromagnetic field [61, 62]. Furthermore, during resonant excitation, the plasmonic metal strongly interacts with incident light. Accordingly, in the photocatalytic process, free electron can easily dephase and create energetic hot electron and holes [63-65]. Therefore, incorporating plasmonic metal with semiconductor is a good way to enlarge the light absorption, charge generation, and separation during the photocatalytic reaction. Recently, because of their excellent combination properties, the noble metal-semiconductor material has a great attention in, water splitting, CO₂ reduction, biosolar cell, hydrogen generation, and photodegradation of pollutant [65-70].

Many efforts have been reported to incorporated new functionalities of plasmonic metal nanoparticles coupling dielectric material, especially Au NPs and TiO₂ [68-73].

The plasmonic golds are common to be used due to their large extinction in visible range wavelength (> 400 nm), while TiO_2 is often used as semiconductor due to their small band gap [71-73]. In the combining Au and TiO_2 , the boundaries such as the shape and size of Au [74] and the oxidation state of TiO_2 [75] play as the important role in the catalytic activity. The Au@TiO_2 in form of core-shells have attracted a great deal due to their unique properties that are not present in either the core or shell but are possible only when the core shell structure exist [63, 72, 73]. As mentioned, the shape of Au can affect the catalytic activity. However, most of them used the spheres Au that showed a narrow-band absorption in a visible region [68-73].

In the case of Au@TiO_2 core-shell, the synthesis route was occur in the ethanol-based solvent [63, 72, 73]. Coincidentally, in the presence of salt in organic solvent (ethanol, DMF), the Au NPs lead to form one-dimensional (1D) chain-like nanostructure [76-78]. This structure has attracted attention because of the great plasmon properties from the coupling effect of their surface plasmon resonance (SPR) [79,80]. Moreover, the SPR is light-harvesting feature from metal that can enhance photocatalytic reaction. Generally, the charge carriers transfer in plasmonic photocatalysis can be explained by the hot electron (e_{hot}^-) injection [81-83]. In this regards, we demonstrated a simple method of synthesis chain-like Au@TiO_2 then compare to isolated Au@TiO_2 for their photocatalytic properties. The investigation of their morphology in affecting the mechanism of catalytic reaction have been discussed. As result, the synergetic enhancement of plasmonic hot electron injection can be driven by strong plasmon coupling effect from neighboring within Au NPs.

Interestingly, the chain-like structure also shows their great photothermal properties. Therefore, the chain-like Au@TiO₂ can greatly enhance the degradation reaction of methylene blue (MB) with various source of light.

III-2. Experimental Section

III-2.1. Material

Gold (III) chloride trihydrate (99.9%), sodium citrate tribasic dehydrate (99.0%), sodium chloride ($\leq 99\%$) and methylene blue (MW 373.90 g/mol) were purchased from Sigma-Aldrich. Solutions of titanium (IV) isopropoxide (Ti[OCH(CH₃)₂]₄, 97%, Sigma-Aldrich) were prepared as a precursor for TiO₂. Ethyl alcohol (99.9%) was purchased from Duksan Co., Korea. All the chemicals were used as received.

III-2.2. Procedure

III-2.2.1. Synthesis of Gold Nanoparticles

Au NPs were synthesized by citrate reduction method. Briefly, 500 mL aqueous solution of HAuCl₄ (0.1 g) was heated until boiling, and 25 mL of sodium citrate solution (0.5 g in 25 mL) was added to the boiling solution. The mixture was further boiled for 15 min with vigorous stirring and then cooled to room temperature. The excess of citrate was eliminated by centrifugation at 9000 rpm for 40 minutes and re-dispersed in DI water.

III-2.2.2. Synthesis of Isolated and Chain-like Au@TiO₂

The precipitated of Au NPs (70 μ L) was added to the ethanolic solution (99.9%, 4mL) for Au NPs and 0.3 mM NaCl ethanolic solution (99.9%, 4 mL) for chain-like Au NPs, respectively. The mixture was allowed to sit for 6 hours. For Au@TiO₂ synthesis, the total volume of the reaction solution was fixed at 4 mL. The titanium tetraisopropoxide (TTIP) in ethanol was added to the ethanolic solution of Au NPs (final concentration of TTIP was 0.325 mM). The reaction sustained for overnight at room temperature without stirring. The ethanolic solution of Au@TiO₂ (1 mL) was then mixed with DI water (3 mL) to prepare for the photocatalytic experiment.

III-2.2.3. Photocatalytic Activity

For the degradation of methylene blue (MB), either isolated Au@TiO₂ (1 mL) or chain-like Au@TiO₂ (1 mL) were added into an aqueous solution of MB (10 mL, 15.4 μ M). The mixture was illuminated under UV-Vis light for 6 hours. For comparison, the degradation of MB was evaluated without light (in dark room), under UV light, and under visible light illumination, respectively. The photocatalytic degradation of MB and kinetical reaction were evaluated with $\ln C/C_0$ at the peak of MB's spectrum.

III-2.3. Measurement

UV-Vis absorbance data were obtained on an Agilent Carry 8454 UV-Visible spectrophotometer. Particle size distribution was evaluated by dynamic light

scattering (DLS) using a Malvern Zetasizer Nano ZS90. Transmission electron microscopy (TEM) was carried out with the Hitachi H-7500 instrument operating at 80 kV. Samples for TEM were prepared by drying a drop of Au@TiO₂ solution onto a carbon-coated copper grid at room temperature. The photocatalytic activity of Au@TiO₂ was evaluated by the degradation of methylene blue (MB) with the light source of LS-150W Xe Arc Lamp (ABET Technologies) at ambient temperature with various cut-off filter. Temperature was measured using thermocouple ST-9234T.

III-3. Results and Discussion

III-3.1. Linear Aggregation of Gold Nanoparticle

The synthesis route of chain-like Au@TiO₂ that is depicted in Figure 9, which has two general steps. First, the growth of chain-like Au NPs was induced by adding organic solvent into the precipitated Au NPs in the presence of NaCl. Second, a TiO₂ layer was coated outside the surface of Au NPs by adding TTIP as precursor. Herein, we describe more detail process of synthesis chain-like Au@TiO₂. In our system, we used citrate ions as reducing and stabilizing agent of Au NPs which produce spherical nanoparticle. The centrifugation process (9000 rpm, 40min) was performed twice including carefully rinsing using DI water to purify gold colloid from byproduct, such as excess citrate and sodium ions. The aqueous supernatant contains sodium ions (from trisodium citrate) and chloride ions (from HAuCl₄) could be directly induce the aggregation of Au NPs in organic solution. Therefore, in this step, the rinsing of

nanoparticle was important. In studying the photocatalytic effect, Au NPs were incubated in ethanol solution without and with NaCl for 6h. For isolated Au NPs, the extinction in the UV-vis spectra of purified particle showed a narrow absorbance at 520 nm as shown in Figure 10a. The spectrum of Au NPs is attributed to the surface plasmon resonance (SPR) band of monodisperse nanoparticle. The incubated Au NPs in ethanol solution without NaCl exhibit there is no changed spectrum after 6h. It indicates the structure of Au NPs was stable in ethanol solution. The structure of this particle was showed at the TEM Image (Figure 10b) in the form of isolated Au NPs having 12 nm of diameter. While, for the case of chain-like Au NPs, the linear aggregation of Au NPs solution was induce by adding the amount of salt (NaCl) in the organic(ethanol)-based solution. As reported, the formation of aggregations Au NPs in ethanol solution can be mainly attributed to the presence of salt. Otherwise, the significant difference in UV-vis spectra of Au NPs incubated ethanol solution in the presence of NaCl was observed in Figure 10c. A new extinction of above 600 nm elaborates into a band upon increasing incubation time. Accordingly the plasmon resonance absorption of the aggregates would have an additional long wavelength component in the optical spectrum relative to the extinction from isolated nanoparticle in solution [84]. Therefore, in this system, the linear aggregation of Au NPs was propped by the longitudinal absorption. Adjusting the concentration of salt and incubation time could control the degree of aggregation [77]. Practically, the incubation time and concentration of NaCl was kept at 6h and 0.3 mM, respectively. At this concentration, there is no change the spectrum of Au NPs after 6h that

indicating fixed form of Au NPs aggregation process. As shown in the TEM image (Figure 10d), the Au NPs is closely linked with other into chain-like assemblies.



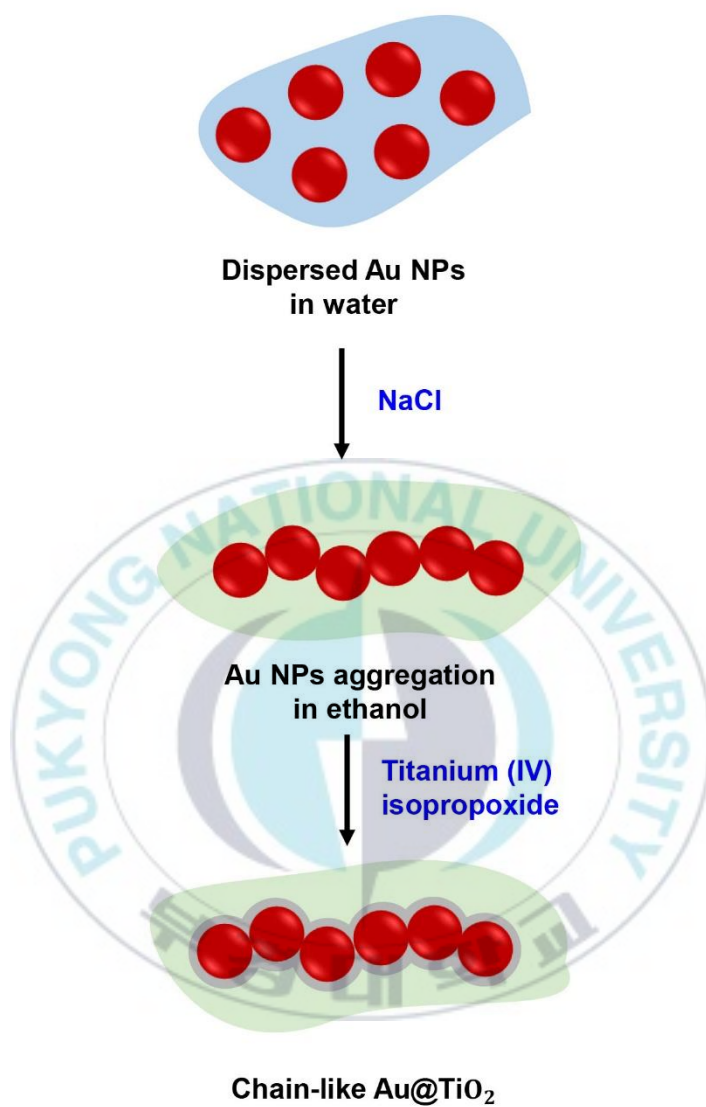


Figure 9. Synthesis route of chain-like Au@TiO₂ structure

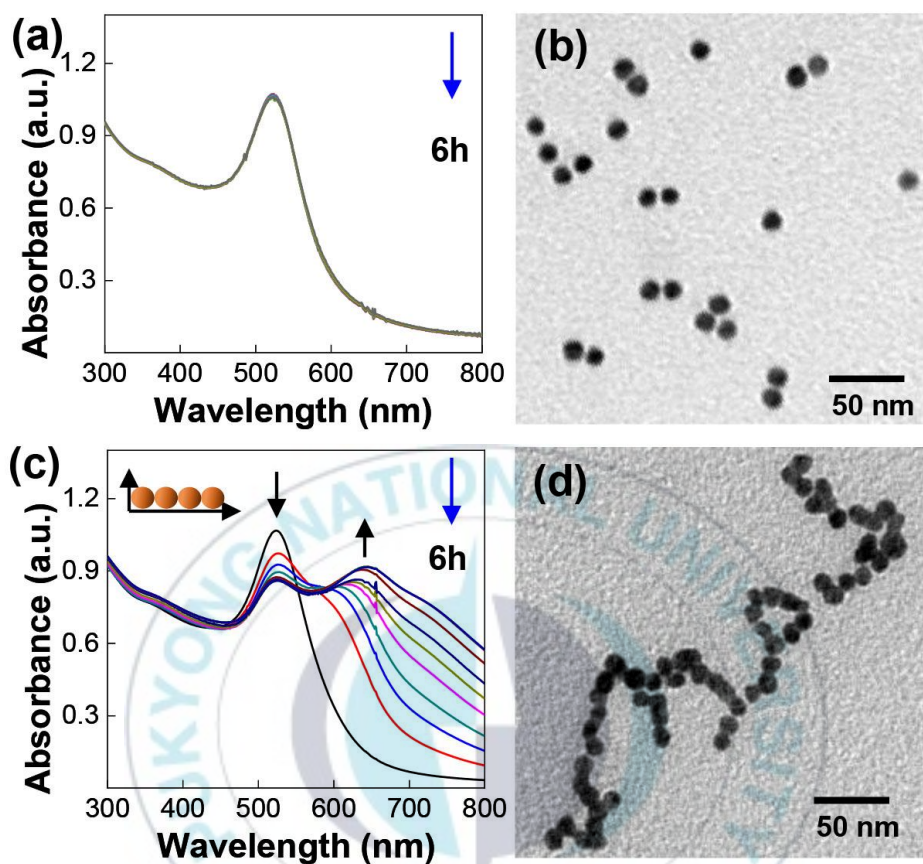


Figure 10. The UV-Vis spectra of Au NPs aggregates formation under different experimental condition: (a) without and (c) with NaCl in ethanol, where the incubation time was 6 hours. TEM Images of Au NPs (b) isolated and (d) chain-like of Au NPs.

III-3.2. Synthesis and Characteristic of Isolated and Chain-like Au@TiO₂

The coating of TiO₂ on the surface of Au NPs step was described. Experimentally, TTIP solution diluted in ethanol. For the synthesis Au@TiO₂, the concentration of gold and TTIP, on the shape of isolated and chain-like were same, 5.3 nM and 0.3 mM, respectively. The UV-Vis extinction of material was displayed in Figure 11a. The Au NPs in ethanol exhibited an LSPR peak in the visible region. During coating of TiO₂, the increasing of refractive index of dielectric environment around of gold nanoparticle was happened. Consequently, after adding titanium precursor, the extinction of isolated and chain-like Au NPs appeared on the red shift of the spectrum, compared to original state. Correspondingly, as shown in inserted photo (Figure 11a), the colour of the Au NPs solution turned from ruby (i) into light purple (ii) for isolated and dark blue (iii) for chain-like of Au@TiO₂, respectively. The representative TEM image of isolated Au@TiO₂ core-shell nanoparticle is shown in Figure 11b. It is clearly seen that the 12 nm-Au NPs cores uniformly coated by the shell of titania having a thickness ~5.5 nm. The total diameter size was comparable with the diameter measured by dynamic light scattering as shown in Figure 11c (ca 23.35 nm). While, for the chain-like Au@TiO₂, TEM image in Figure 11d shows the long chain-like Au NPs which cover by TiO₂ having comparable thickness with isolated shape. The size of nanoparticle also measure with DLS that obtained average size of 90.53 nm (Figure 11e). It indicates the length of chain-like Au@TiO₂. In our study, the varying number of Au NPs in a chain of Au@TiO₂ were obtained. However, without the controlling

of number the Au NPs, we still can investigate the effect of their morphology compare to the isolated ones.



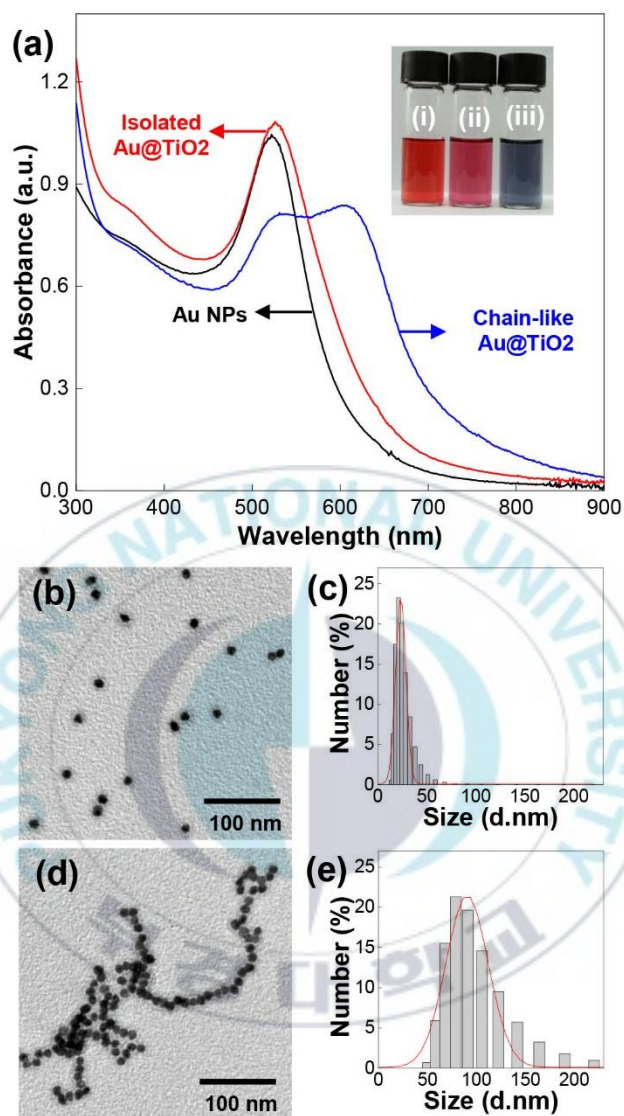


Figure 11. (a) The UV-Vis spectra of Au NPs (black color), isolated Au@TiO₂ (red color), and chain-like Au@TiO₂ (blue color) including digital photo of Au NPs (i), isolated Au@TiO₂ (ii), and chain-like Au@TiO₂ (iii), respectively. TEM Images and DLS histograms of (b-c) isolated and (c-d) chain-like of Au@TiO₂, respectively.

III-3.3. Photocatalytic Activity

For investigation the effect of the chain-like Au@TiO₂ to their photocatalytic activity, we applied this structure to dye degradation reaction and compare to isolated Au@TiO₂. In detail, the dyes can act as the organic pollutants in aquatic system. However, the Au@TiO₂ in our system was difficult to redisperse in water without changing structure. Therefore, in our study, we mix the Au@TiO₂ ethanol-based with DI water in ratio 1:3 (v/v). Using this condition, we can maintain the structure. This mixture was stable that proved with UV-Vis spectra, size distribution and TEM image. At Figure 12a, the UV-Vis spectra of isolated Au@TiO₂ was stable until 6 day. This structure also shown in size distribution (Figure 12b-d). Moreover, the TEM image was exhibited in Figure 12e. This condition also obtain in the form of chain-like structure (Figure 13a-e).

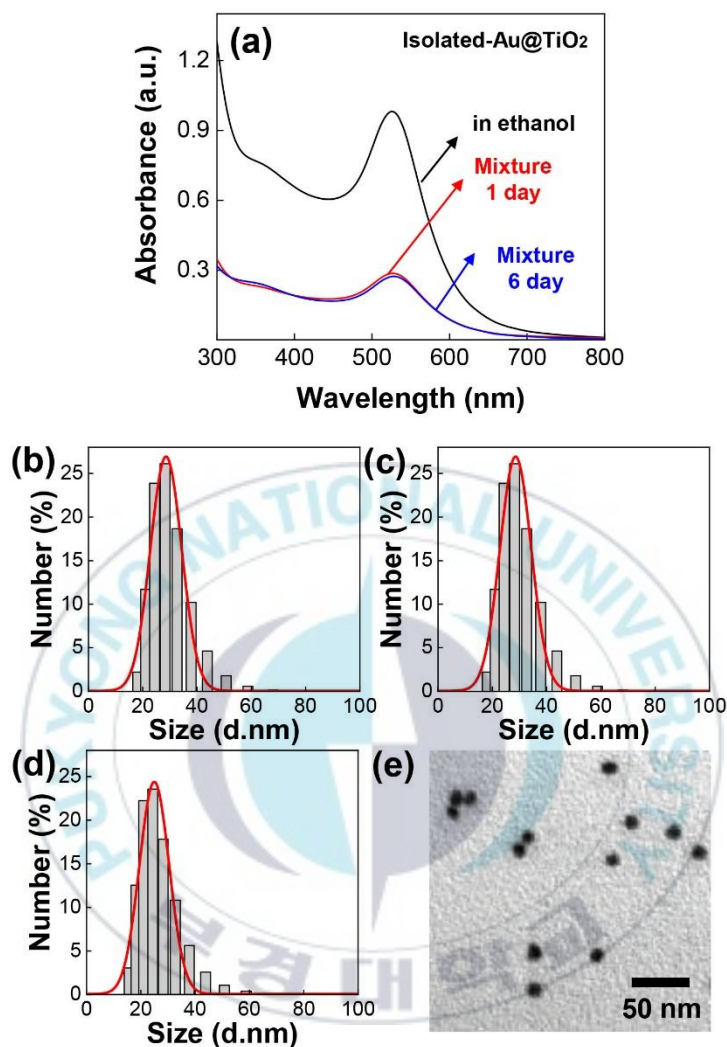


Figure 12. (a) The UV-Vis spectra of isolated Au@TiO₂ in ethanol (black color), in mixture 0 day (red color), and in mixture 6 day (blue color). Size distribution of isolated Au@TiO₂ in (b) ethanol, (c) mixture 1 day and (d) mixture 6 days. (e) TEM image of mixture isolated Au@TiO₂.

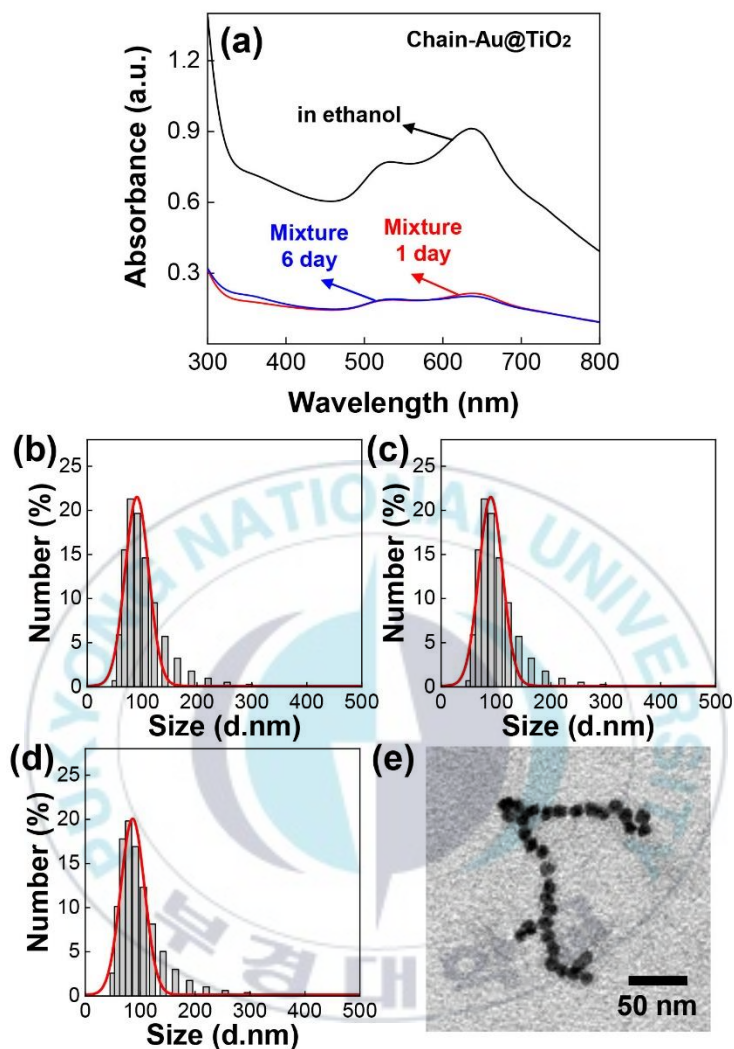
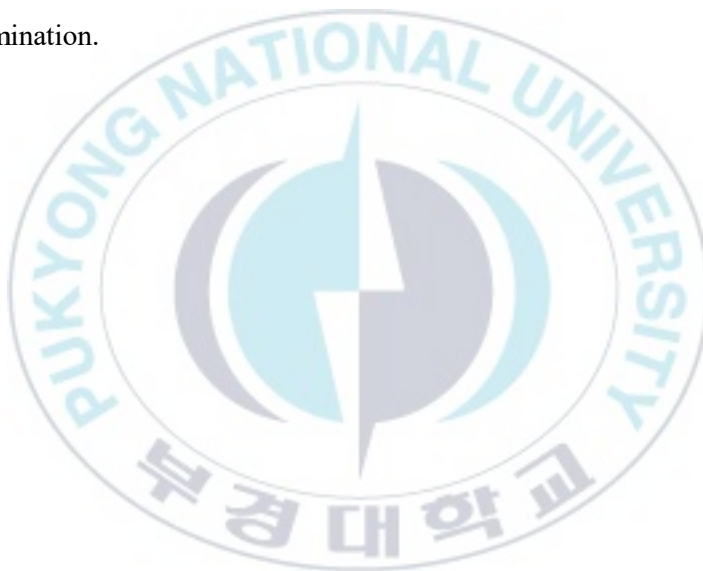


Figure 13. (a) The UV-Vis spectra of chain-like Au@TiO₂ in ethanol (black color), in mixture 0 day (red color), and in mixture 6 day (blue color). Size distribution of chain-like Au@TiO₂ in (b) ethanol, (c) mixture 1 day and (d) mixture 6 days. (e) TEM image of mixture chain-like Au@TiO₂.

For the purpose, the prepared 1 mL of mixture Au@TiO₂ was placed into 10 mL aqueous of methylene blue (MB). As reported, there are two major absorption band in aqueous methylene blue, at 293 nm ($\pi - \pi^*$) and 664 nm ($n - \pi^*$) [85]. Consequently, MB dye can harvest the solar photon in the UV and visible range, while the TiO₂ only absorbs UV light and Au NPs only absorbs visible light. Then, to examine the synergetic interaction between gold and the TiO₂, we used various source light, UV light, visible light and UV-Vis light. For those conditions, the solar simulator was operated using cut-off filter, IR filter + 400 nm short-pass filter, IR filter + 400 nm long-pass filter and only IR filter, respectively. The spectrum of the MB degradation were collected and shows in Figure 14a-d and 15a-d, for isolated and chain-like structure, respectively. First, we monitored the-time dependent absorption of MB at 664 nm under dark condition. Without illumination, either using isolated Au@TiO₂ or chain-like Au@TiO₂ of mixture, the spectra band absorption at 664 nm were constant (Figure 14a and 15a). It indicates that without light, the catalytic reaction cannot occur. Hereafter, using identical concentration of catalyst (isolated and chain-like of Au@TiO₂) and concentration of MB solution, the mixture were illuminated in various illumination as previous described. In all the condition illumination, the MB absorbance at 664 nm decreased with time in various rate (figure 5c-d and 6c-d). For simply, we summaries the photocatalytic performance of isolated and chain-like of Au@TiO₂ in Figure 16a. In this figure, the quantitative analysis was showed. The peak absorbance of 664 nm MB was fitted by using first order kinetic equation, which is $(C/C_0) = -kt$, where C_0 and C are the concentration of

MB molecules at initial and given time t , respectively, and k is the rate constant. From the fitted line, the rate constant of degradation reaction can be obtained. Therefore, the rate of catalytic were exhibited as statistic histogram in Figure 16b. Since the concentration of Au NPs and TiO_2 that used were same, the Figure 16b shows that the chain-like morphology of Au@TiO_2 can enhance the photocatalytic activity in all illumination condition compare to isolated ones. Furthermore, either isolated or chain-like morphology have value of rate constant with comparison $\text{UV-Vis} > \text{UV} > \text{visible illumination}$.



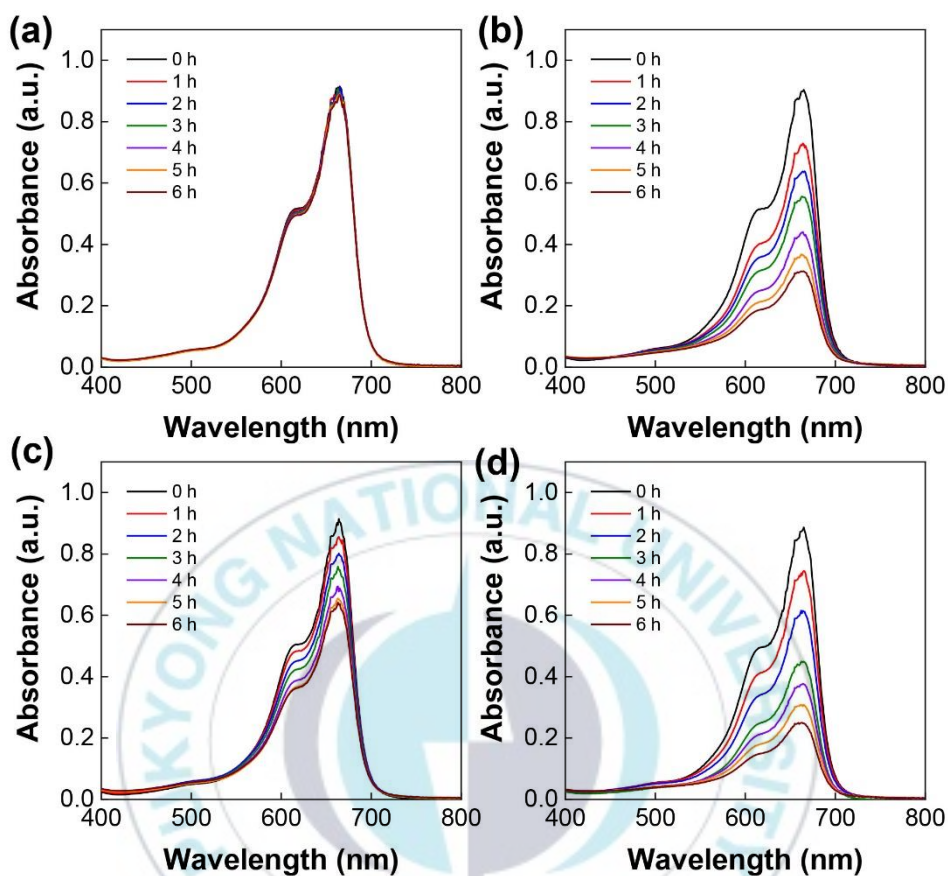


Figure 14. The UV-Vis spectrum of Methylene Blue degradation using isolated Au@TiO₂ under (a) dark condition, (b) UV, (c) visible and (d) UV-visible illumination.

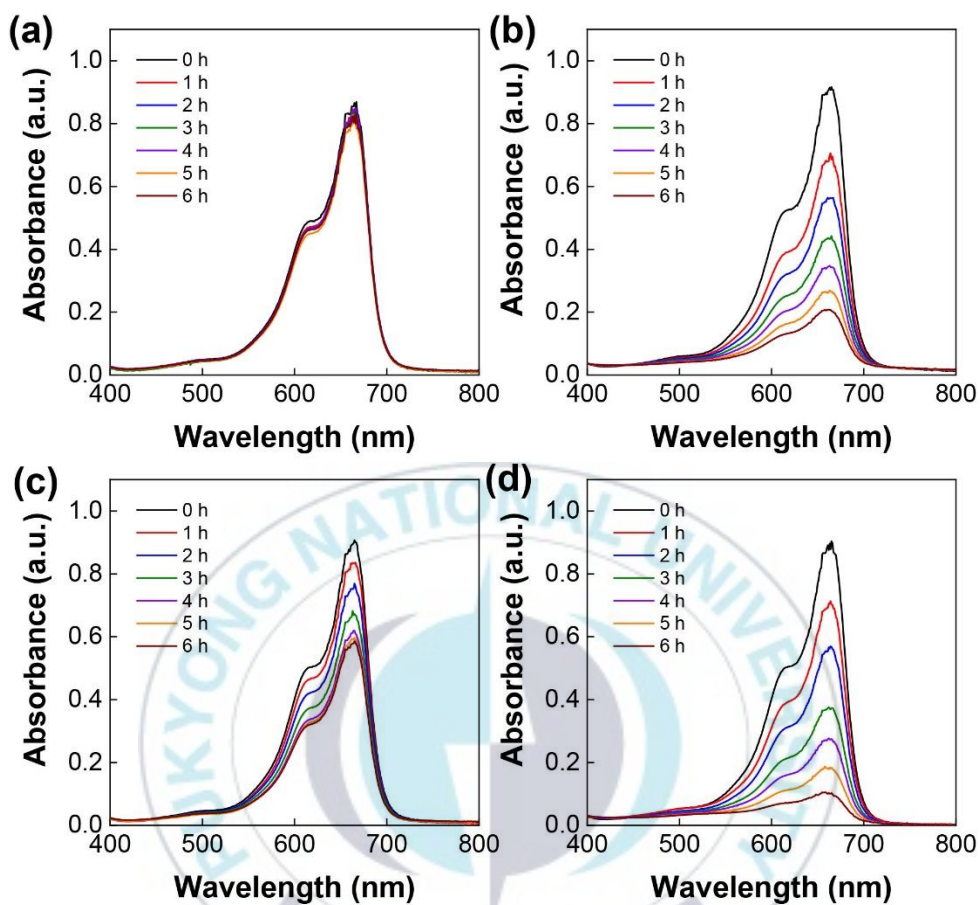


Figure 15. The UV-Vis spectrum of Methylene Blue degradation using chain-like Au@TiO₂ under (a) dark condition, (b) UV, (c) visible and (d) UV-visible illumination.

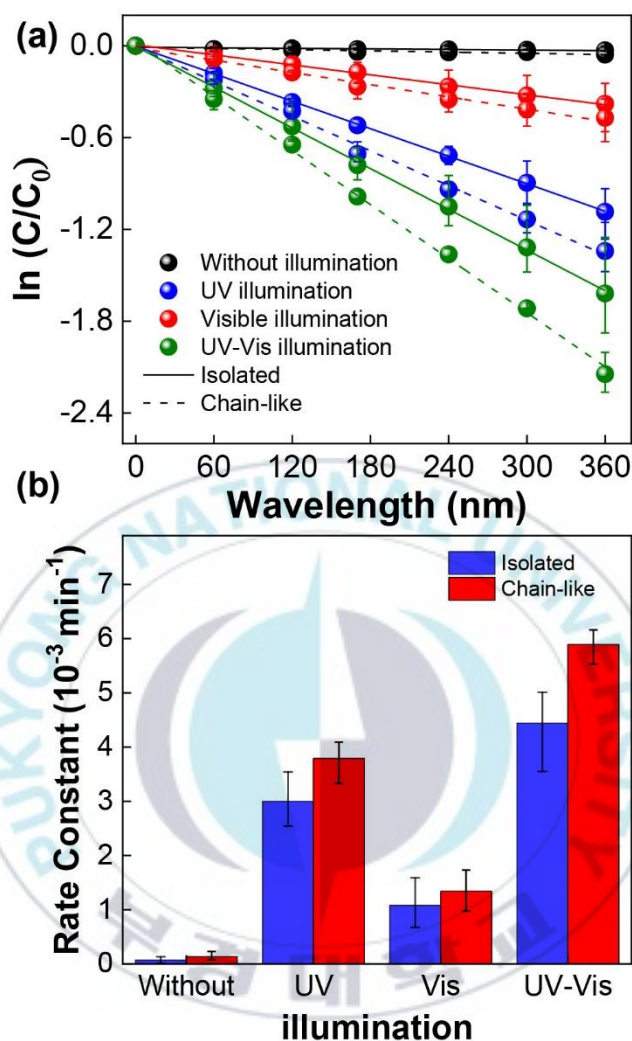


Figure 16. (a) Time-dependent absorbance values at 664 nm in the time course of MB photocatalytic decomposition from isolated (straight line) and chain-like (dash line) of Au@TiO₂ without (black color), UV (blue color), visible (red color) and UV-Visible (green color) light illumination, respectively. (b) The statistic histogram of photocatalytic rate constant of isolated (blue color) and chain-like (red color) of Au@TiO₂.

For describe the trends of the photocataytic performance in our study, the possible pathway of MB degradation was depicted in Figure 17a. The metal-semiconductor has synergetic contribution for degradation MB. For instance, under UV illumination, in the presence of metal, the contact of TiO_2 and Au NPs creates Schottky junction that can facilitate charge separation leading to suppress the electron-hole recombination. In this case, the Au provides a fast lane for charge transfer, and the surface of Au can act as a charge-trap center giving more active sites for photoreaction. Hereafter, under visible illumination, the electron from Au can transfer to TiO_2 . In general, plasmonic metal can excite the charge carriers in semiconductor through plasmonic-induced resonance energy transfer (PIRET) and hot electron injections processes. However, for the case of Au@TiO_2 core-shell, there is no overlap spectral between Au and TiO_2 , consequently hot electron injection dominantly contribute in the charge transfer [63]. Therefore the hot electron created by absorbing visible light of Au NPs. Then, the hot electron injected into TiO_2 conductive band (CB). After completely charge separation, the Au@TiO_2 interfaces provides the oxidation and reduction reaction, promoting photocatalysis activity. As result, the photocatalytic of chain-like has better performance compare to isolated ones. Especially under visible illumination, only Au NPs has contribution in degradation of dyes. In this condition, photocatalytic activity of the chain-like structure shows greater performance. It indicate the morphology of plasmonic metal affects the hot electron injection process. The chain-like structure has strongly plasmon coupling. The couple of this metal nanoparticle show two absorption peak.

It can extract the energy from dipole radiation and reduce the radioactive scattering [21]. Consequently, it can enhance the photocatalytic activity. In addition, the synergetic effect of plasmon coupling has been demonstrated to greatly extend the light harvest and easily promote fast hot electron injection [64].

Since the plasmon coupling of the neighboring NPs within Au chain leads to the red shift, we expected that the chain-like morphology could improve the photothermal performance under light irradiation. For this purpose, we illuminated both of catalysts with UV-visible light as shown in Figure 17b. To make sure the photothermal effect, we also compared to the solvent of catalyst, which is ethanol. The temperature of ethanol gradually increased with time. However, the different temperatures reached only 2.2°C. The different temperature is smaller compared to Au@TiO₂ having 5.2°C for isolated and 7.4°C for chain-like. Therefore, we can still consider that there is a photothermal effect in their morphology. Furthermore, as expected, the increment in temperature of chain-like Au@TiO₂ was higher than the isolated one. In the dye degradation, the photo-excitation creates the thermal energy (heat) that affects the transportation of photogenerated carriers on the system. Where the heating up of surrounding environment can increase the redox reaction rates and the mass transfer. Therefore, the photothermal properties can improve the photocatalytic activity. Consequently, the chain-like Au@TiO₂ has higher photocatalytic performance.

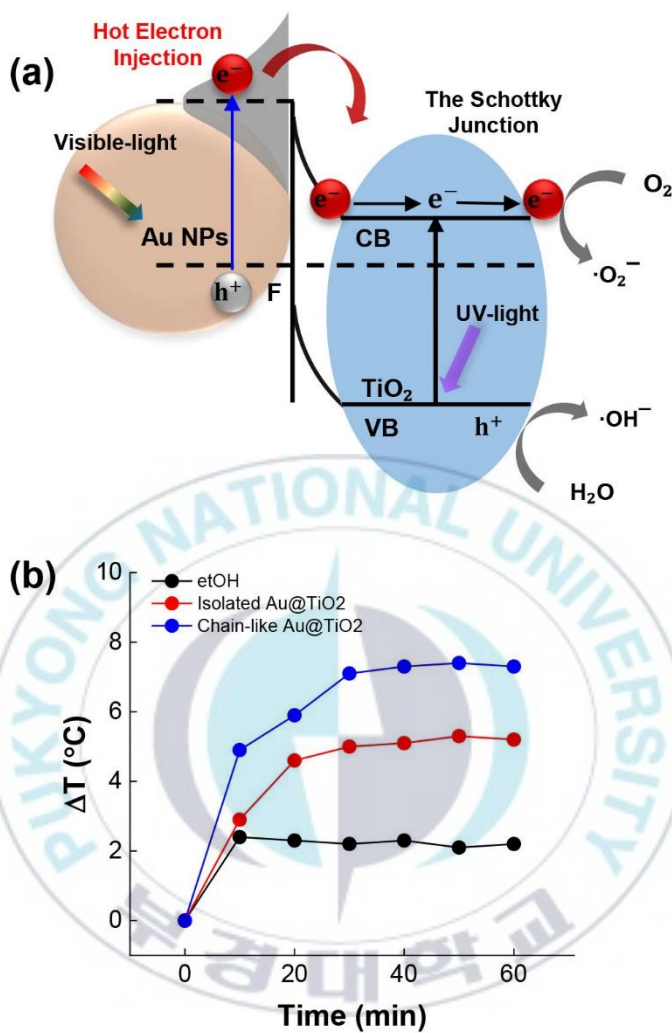


Figure 17. (a) Schematic illustration of MB degradation over Au@TiO₂. (b) Photothermal of isolated (red color) and chain-like (blue color) of Au@TiO₂

III-4. Conclusion

In this regard, we have been demonstrated the chain-like nanoparticle assembly to investigate the effects of their morphologies on the plasmon-assisted catalytic activities. The chain-like Au NPs were synthesized by adding the amount of salt. The Au@TiO₂ core-shell NPs were synthesized by controlled hydrolysis of TiO₂ precursor around the surface of Au NPs. The prepared Au@TiO₂ NPs chain-like assemblies lead to interesting materials properties in photocatalytic reaction. By illuminating the synthesized Au@TiO₂ NPs with different-colored light, we investigated the synergistic effect of Au and TiO₂ on the degradation kinetics of methylene blue. Interestingly, the chain-like structure shows enhance photocatalytic performance compare to isolated ones.

References

- [1] X. Tang, X. Wang, R. Cattley, F. Gu and A. D. Ball (2018), *Sensors*, **18**, 4113.
- [2] Z. L. Wang (2014), *Faraday Discuss.*, **176**, 447.
- [3] S. Niu, S. Wang, L. Lin, Y. Liu, Y. S. Zhou, Y. Hu and Z. L. Wang (2013), *Energy Environ. Sci.*, **6**, 3576.
- [4] J. Chen and Z. L. Wang (2017), *Joule*, **1**, 480.
- [5] F. R. Fan, L. Lin, G. Zhu, W. Wu, R. Zhang and Z. L. Wang (2012), *Nano Lett.*, **12**, 3109.
- [6] J. Chen, G. Zhu, W. Yang, Q. Jing, P. Bai, Y. Yang, T. C. Hou and Z. L. Wang (2013), *Adv. Mater.*, **25**, 6094.
- [7] P. Bai, G. Zhu, Z. H. Lin, Q. Jing, J. Chen, G. Zhang, J. Ma and Z. L. Wang (2013), *ACS Nano*, **7**, 3713.
- [8] S. H. Shin, Y. H. Kwon, Y. H. Kim, J. Y. Jung, M. H. Lee and J. Nah (2015), *ACS Nano*, **9**, 4621.
- [9] H. Y. Li, L. Su, S. Y. Kuang, C. F. Pan, G. Zhu and Z. L. Wang (2015), *Adv. Funct. Mater.*, **25**, 5691.
- [10] P. Xue, Q. Li, Y. Li, L. Sun, L. Zhang, Z. Xu and Y. Kang (2017), *ACS Appl. Mater. Interfaces*, **9**, 33632.
- [11] Y. Jin Chuah, Y. T. Koh, K. Lim, N. V. Menon, Y. Wu and Y. Kang (2015), *Sci. Rep.*, **5**, 18162.

- [12] I. You, T. G. Lee, Y. S. Nam and H. Lee (2014), *ACS Nano*, **8**, 9016.
- [13] J. H. Waite (1987), *Int. J. Adhesion and Adhesives*, **7**, 9.
- [14] D. R. Dreyer, D. J. Miller, B. D. Freeman, D. R. Paul and C. W. Bielawski (2012), *Langmuir*, **28**, 6428.
- [15] H. Lee, S. M. Dellatore, W. M. Miller and P. B. Messersmith (2007), *Science*, **318**, 426.
- [16] K. L. Kelly, E. Coronado, L. L. Zhao and G. C. Schatz (2003), *J. Phys. Chem. B.*, **107**, 668.
- [17] Y. Xia, Y. Xiong, B. Lim and S. E. Skrabalak (2009), *Angew. Chem. Int. Ed.*, **48**, 60.
- [18] E. Hutter and J. H. Fendler (2004), *Adv. Mater.*, **16**, 1689.
- [19] S. Link and M. A. El-Sayed (1999), *J. Phys. Chem. B.*, **103**, 8410.
- [20] E. A. Coronado, E. R. Encina and F. D. Stefani (2011), *Nanoscale*, **3**, 4042.
- [21] X. Zhang, Y. L. Chen, R. S. Liu and D. P. Tsai (2013), *Rep. Prog. Phys.*, **76**, 046401.
- [22] K. Hashimoto, H. Irie and A. Fujhisima (2005), *Jpn. J. Appl. Phys.*, **44**, 8269.
- [23] I. Thomann, B. A. Pinaud, Z. Chen, b. M. Clemens, T. F. Jaramillo and M. L. Brongersma (2011), *Nano Lett.*, **11**, 3440.
- [24] Z. C. Wu, Y. Zhang, T. x. Tao, L. Zhang and H. Fong (2010), *Applied Surface Science*, **257**, 1092.

- [25] A. S. Castillo, M. C. Hermo, B. R. González, M. P. Lorenzo, Z. Wang, X. T. Kong, A. O. Govotov and M. A. C. Duarte (2016), *J. Phys. Chem. C*, **120**, 11690.
- [26] C. Clavero (2014), *Nature Photonics*, **8**, 95.
- [27] T. P. White and K. R. Catchpole (2012), *Appl. Phys. Lett.*, **101**, 073905.
- [28] Y. Nishijima, K. Ueno, Y. Yokota, K. Murakoshi and H. Misawa (2010), *J. Phys. Chem. Lett.*, **1**, 2031.
- [29] S. Chu and A. Majumdar (2012), *Nature*, **488**, 294.
- [30] Z. L. Wang, J. Chen and L. Lin (2015), *Energy Environ. Sci.*, **8**, 2550.
- [31] Y. Yang, H. Zhang, Z. H. Lin, Y. S. Zhou, Q. Jing, Y. Su, J. Yang, J. Chen, C. Hu and Z. L. Wang (2013), *ACS Nano*, **7**, 9213.
- [32] A. Chandrasekhar, N. R. Alluri, B. Saravanakumar, S. Selvarajan and S. J. Kim (2016), *ACS Appl. Mater. Interfaces*, **8**, 9692.
- [33] Z. H. Lin, G. Zhu, Y. S. Zhou, Y. Yang, P. Bai, J. Chen and Z. L. Wang (2013), *Angew. Chem. Int. Ed.*, **52**, 5065.
- [34] G. Zhu, C. Pan, W. Guo, C. Y. Chen, Y. Zhou, R. Yu and Z. L. Wang (2012), *Nano Lett.*, **12**, 4960.
- [35] T. Zhou, C. Zhang, C. B. Han, F. R. Fan, W. Tang and Z. L. Wang (2014), *ACS Appl. Mater. Interfaces*, **6**, 14695.
- [36] T. Zhou, L. Zhang, F. Xue, W. Tang, C. Zhang and Z. L. Wang (2016), *Nano Res.*, **9**, 1442.

- [37] W. Tang, C. B. Han, C. Zhang and Z. L. Wang (2014), *Nano Energy*, **9**, 121.
- [38] C. Zhang, T. Zhou, W. Tang, C. Han, L. Zhang and Z. L. Wang (2014), *Adv. Energy Mater.*, **4**, 1301798.
- [39] J. Chen, J. Yang, Z. Li, X. Fan, Y. Zi, Q. Jing, H. Guo, Z. Wen, K. C. Pradel, S. Niu and Z. L. Wang (2015), *ACS Nano*, **9**, 3324.
- [40] L. M. Zhang, C. B. Han, T. Jiang, T. Zhou, X. H. Li, C. Zhang and Z. L. Wang (2016), *Nano Energy*, **22**, 87.
- [41] T. Jiang, L. M. Zhang, X. Chen, C. B. Han, W. Tang, C. Zhang, L. Xu and Z. L. Wang (2015), *ACS Nano*, **9**, 12562.
- [42] L. Xu, Y. Pang, C. Zhang, T. Jiang, X. Chen, J. Luo, W. Tang, X. Cao and Z. L. Wang (2017), *Nano Energy*, **31**, 351.
- [43] Z. L. Wang (2013), *ACS Nano*, **7**, 9533.
- [44] H. J. Yoon, H. Ryu and S. W. Kim (2018), *Nano Energy*, **51**, 270.
- [45] C. F. Gallo and W. L. Lama (1976), *Journal of Electrostatics*, **2**, 145.
- [46] R. Huang and J. Zhu (2017), *RSC Adv.*, **7**, 49562.
- [47] K. Y. Lee, J. Chun, J. H. Lee, K. N. Kim, N. R. Kang, J. Y. Kim, M. H. Kim, K. S. Shin, M. K. Gupta, J. M. Baik and S. W. Kim (2014), *Adv. Mater.*, **26**, 5037.
- [48] J. Chun, J. W. Kim, W. S. Jung, C. Y. Kang, S. W. Kim, Z. L. Wang and J. M. Baik (2015), *Energy Environ. Sci.*, **8**, 3006.

- [49] S. Wang, Y. Zi, Y. S. Zhou, S. Li, F. Fan, L. Lin and Z. L. Wang (2016), *J. Mater. Chem. A*, **4**, 3728.
- [50] Q. Jiang, B. Chen, K. Zhang and Y. Yang (2017), *ACS Appl. Mater. Interfaces*, **9**, 43716.
- [51] J. Chen, H. Guo, X. He, G. Liu, H. Shi and C. Hu (2016), *ACS Appl. Mater. Interfaces*, **8**, 736.
- [52] D. Kim, S. J. Park, S. B. Jeon, M. L. Seol and Y. K. Choi (2016), *Adv. Electron. Mater.*, **2**, 1500331.
- [53] S. J. Choi, T. H. Kwon, H. Im, D. I. Moon, D. J. Baek, M. L. Seol, J. P. Duarte and Y. K. Choi (2011), *ACS Appl. Mater. Interfaces*, **3**, 4552.
- [54] D. Sharma, W. Jia, F. Long, S. Pati, Q. H. Chen, Y. Qyang, B. P. Lee, C. K. Choi and F. Zhao (2019), *Bioactive Materials*, **4**, 142.
- [55] J. G. Rivera, R. Iglio, G. Barillaro, C. Duce and M. R. Tine (2018), *Polymers*, **10**, 616.
- [56] A. Thakur, S. Ranote, D. Kumar, K. K. Bhardwaj, R. Gupta and G. S. Chauhan (2018), *ACS Omega*, **3**, 7925.
- [57] R. Simpkin (2010), *IEEE Trans. Microwave Theory Tech*, **58**, 545.
- [58] J. Wang, Y. Xie, J. Liu, Z. Zhang, Q. Zhuang and J. Kong (2018), *Polymers*, **10**, 1349.
- [59] W. Ni, X. Kou, Z. Yang and J. Wang (2008), *ACS. Nano*, **2**, 677.
- [60] D. M. Schaadt, B. Feng and E. T. Yu (2005), *Appl. Phys. Lett.*, **86**, 063106.

- [61] W. Tu, Y. Zhou, H. Li, P. Li and Z. Zou (2015), *Nanoscale*, **7**, 14232.
- [62] S. K. Cushing, J. Li, F. Meng, T. R. Senty, S. Suri, M. Zhi, M. Li, A. D. Bristow and N. Wu (2012), *J. Am. Chem. Soc.*, **134**, 15033.
- [63] S. K. Cushing, J. Li, J. Bright, B. T. Yost, P. Zheng (2015), A. D. Bristow and N. Wu, *J. Phys. Chem.*, **119**, 16239.
- [64] W. Cheng, H. Su, F. Tang, W. Che, Y. Huang, X. Zheng, T. Yao, J. Liu, Y. Jiang and Q. Liu (2017), *J. Mater. Chem. A.*, **5**, 19649.
- [65] C. Le, H. Choi, I. I. Nedrygailov, Y. K. Lee, S. Jeong and J. Y. Park (2018), *ACS. Appl. Mater. Interfaces*, **10**, 5081.
- [66] L. Du, G. Shi, Y. Zhao, X. Chen, H. Sun, F. Liu, F. Chen and W. Xie (2019), *Chem. Sci.*, **10**, 9650.
- [67] K. Sekizawa, K. Maeda, K. Domen, K. Koike and O. Ishitani (2013), *J. Am. Chem. Soc.*, **135**, 4596.
- [68] Y. Yang, H. B. Gobeze, F. D. Sauza, R. Jankowiak and J. Li (2016), *Adv. Mater. Interfaces*, **3**, 1600371.
- [69] Z. W. Seh, S. Liu, M. Low, S. Y. Zhang, Z. Liu, A. Mlayah and M. Y. Han (2012), *Adv. Mater.*, **24**, 2310.
- [70] I. M. Arabatzis, T. Stergiopoulos, D. Andreeva, S. Kitova, S. G. Neophytides and P. Falaras (2013), *Journal of Catalysis*, **220**, 127.
- [71] H. Li, Z. Bian, J. Zhu, Y. Huo, H. Li and Y. Lu (2007), *J. Am. Chem. Soc.*, **129**, 4538.

- [72] W. L. Liu, F. C. Lin, Y. C. Yang, C. H. Huang, S. Gwo, M. H. Huang and J. S. Huang (2013), *Nanoscale*, **5**, 7953.
- [73] A. Pougin, G. Dodekatos, M. Dilla, H. Tuyuz and J. Strunk (2018), *Chem. Eur. J.*, **24**, 1.
- [74] M. S. Chen and D. W. Goodman (2006), *Catal. Today*, **111**, 22.
- [75] M. Commoti, W. C. Li, B. Spliethoff and F. Schuth (2006), *J. Am. Chem. Soc.*, **128**, 917.
- [76] X. Han, J. Goebel, Z. Lu and Y. Yin (2011), *Langmuir*, **27**, 5282.
- [77] M. Yang, G. Chen, Y. Zhao, G. Silber, Y. Wang, S. Xing, Y. Han and H. Chen (2010), *Phys. Chem. Chem. Phys.*, **12**, 11850.
- [78] Z. Lin, W. Zhang, Q. Fu, H. Yue, W. Wei, P. Tang, W. Li, W. Li, L. Lin, G. Ma and D. Ma (2014), *small*, **10**, 3619.
- [79] S. Lin, M. Li, E. Dujardin, C. Girard and S. Mann (2005), *Adv. Mater.*, **17**, 2553.
- [80] Y. Ofir, B. Samanta and V. M. Rotello (2008), *Chem. Soc. Rev.*, **37**, 1814.
- [81] A. Furube, L. Du, K. Hara, R. Katoh and M. Tachiya (2007), *J. Am. Chem. Soc.*, **129**, 14852.
- [82] Y. K. Lee, C. H. Jung, J. Park, H. Seo, G. A. Somorjai and J. Y. Park (2011), *Nano Lett.*, **11**, 4251.
- [83] Y. Shiraishi, N. Yasumoto, J. Imai, H. Sukamoto, S. Tanaka, S. Ichikawa, B Ohtani and T. Hirai (2017), *Nanoscale*, **9**, 8349.

- [84] P. Galletto, P. F. Brevet, H. H. Girault, R. Antonie and M. Broyer (1999),
J. Phys. Chem. B, **103**, 8760.
- [85] D. Heger, J. Jirkovský and P. Klán (2005), *J. Phys. Chem. A*, **109**, 6702.



Acknowledgements

From the writing of this thesis, I have received a great assistance and support. I would first like to thank my advisor, Professor Seong Il Yoo whose proficiency was invaluable in the directing of the research topic in particular. All of your opportunities which given me to create interesting idea in the field of scientific, It could improve my hard skills. Moreover, your sharing knowledge will be very useful for my future. Because of you, I could complete all of my research activity.

Next, I would like to thank my parent and my brother for a nice counsel that always there for me. I could strengthen my mental and my physical from your big supporting. You told me that I certainly achieved my dream, even I got into trouble.

In addition, I would also like to thank all of my friends who I meet here in Busan. You were given me happiness to rest my feels outside of my research activity. Finally I would like to thank the members of the “Self Assembly Nanomaterial” group both past and present: Molly, Song Chang Hyun, Limpat, Gu Ja Min and Lee Geon Seok for your help and support.

Pukyong National University, Busan, South Korea

February 2020

Merreta Noorenza Biutty